Coordination Chemistry Reviews, 99 (1990) 213–252
Elsevier Science Publishers B.V., Amsterdam – Printed in The Netherlands

SPECTROSCOPIC AND PHOTOCHEMICAL PROPERTIES OF d^{10} METAL COMPLEXES

CHARLES KUTAL

Department of Chemistry, University of Georgia, Athens, GA 30602 (U.S.A.)

(Received 15 June 1989)

CONTENTS

ABBREVIATIONS

bipy	2,2′-bipyridine
CTTS	charge transfer to solvent
dba	dibenzylideneacetone
diphos	1,2-bis(diphenylphosphino)ethane
6,6′-dmbp	6,6′-dimethyl-2,2′-bipyridine
dmp	2,9-dimethyl-1,10-phenanthroline
dpp	2,9-diphenyl-1,10-phenanthroline
dppm	bis(diphenylphosphino)methane
dta	dithioacetate

0010-8545/90/$14.00

EDTA	ethylenediaminetetraacetic acid
IL	intraligand
LLCT	ligand-to-ligand charge transfer
LMCT	ligand-to-metal charge transfer
mbp	6-methyl-2,2′-bipyridine
Me	methyl
2-MeTHF	2-methyl-tetrahydrofuran
MLCT	metal-to-ligand charge transfer
MV^{2+}	methylviologen dication
Ph	phenyl
phen	1,10-phenanthroline
pip	piperidine
PPh_3	triphenylphosphine
prophos	1,3-bis(diphenylphosphino)propane
py	pyridine
pza	bis[2-(3,5-dimethyl-1-pyrazolyl)ethyl]amine
quin	quinoline
cis-stil	*cis*-4-stilbazole
trans-stil	*trans*-4-stilbazole
tbaa	tribenzylideneacetylacetone
tdt	3,4-toluenedithiolate
timm	tris[2-(1-methylimidazolyl)]methoxymethane
TMP	1,3,5-trimethylpyrazole
tpp	2,4,7,9-tetraphenyl-1,10-phenanthroline
trpyn	tris[2-(1-pyrazolyl)ethyl]amine
5-X-phen	5-substituted 1,10-phenanthroline
4-X-PhS	4-substituted benzenethiolate

A. INTRODUCTION

There exists an extensive literature dealing with the synthesis, structural characterization and thermal chemistry of coordination compounds containing a d^{10} metal center [1,2]. Because of the completely filled metal *d*-subshell, the electronic ground states of these compounds do not experience the ligand field stabilization effects common to d^{1-9} electronic configurations [3]. Thus neither the coordination number nor the geometric structure of a d^{10} complex is imposed by ligand field requirements. Similarly, activation energies for ligand substitution reactions contain no ligand field contribution.

When considering the excited state properties of metal complexes, we again encounter an important distinction between the d^{1-9} and d^{10} configurations. In the former case, electronic transitions between orbitals of the

partially filled d-subshell give rise to ligand field excited states [4–7]. Since d–d transitions cannot occur in d^{10} complexes, the spectroscopy and photochemistry in these systems are determined solely by the properties of other types of electronic excited states. Studies of d^{10} complexes thus afford the opportunity to obtain information about these other states under circumstances where ligand field effects are minimized.

In this article we review the principal features of the electronic spectroscopy and photochemistry of d^{10} metal complexes. This general area has experienced considerable growth in recent years, particularly with regard to the diversity of metal–ligand combinations examined. To keep the discussion within reasonable limits, we shall focus upon the behavior of discrete, low nuclearity complexes, i.e. those containing four or less metal atoms. Accordingly, the properties of larger d^{10} metal-containing aggregates such as silver halide microcrystals (important in commercial photographic processes [8]) and particulate semiconductors (e.g. ZnS or CdS [9]) are not treated here.

B. SPECTROSCOPIC PROPERTIES

We shall follow the standard practice of describing each electronic state of a metal complex in terms of its dominant molecular orbital configuration and then classifying transitions between states on the basis of the orbitals that undergo a change in electron occupancy [4–7]. This procedure can be

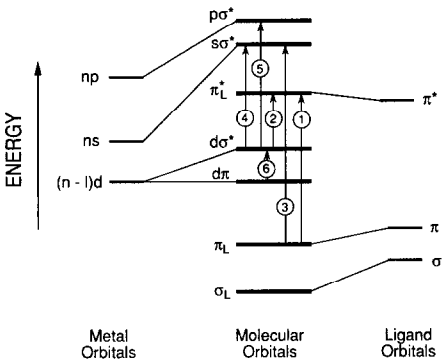

Fig. 1. Schematic energy level diagram of the molecular orbitals and electronic transitions in an octahedral coordination compound. Transition types are (1) intraligand, (2) metal-to-ligand charge transfer, (3) ligand-to-metal charge transfer, (4) interconfigurational metal-centered, $d-s$, (5) interconfigurational metal-centered, $d-p$, (6) ligand field (absent in d^{10} complexes). For simplicity, all orbitals of a given type are represented by a single energy level. It should be noted that the $d\pi$ orbitals may be bonding, non-bonding or antibonding ($d\pi^*$) in character, depending upon the exact metal–ligand combination.

illustrated with the aid of the orbital energy diagram in Fig. 1. Shown in very qualitative fashion are the molecular orbitals that result from mixing the valence orbitals of a transition metal with the appropriate symmetry-adapted orbitals of six ligands disposed at the vertices of an octahedron. If the metal–ligand interaction is weak, the molecular orbitals σ_L, π_L and π_L^* are localized mainly on the ligands whereas $d\pi$, $d\sigma^*$, $s\sigma^*$ and $p\sigma^*$ are predominantly metal in character (the letter descriptors d, s and p designate the specific metal orbital involved).

Transitions between these orbitals give rise to a variety of electronic excited states. A $d\sigma^* \rightarrow \pi_L^*$ transition, for example, involves the promotion of an electron from a metal-centered d-antibonding orbital to a ligand

TABLE 1

Examples of different orbital transition types

Entry	Complex	Solvent	λ_{max} (ϵ) (nm) ($M^{-1}cm^{-1}$)	Orbital assignment	Ref.
a	$Ag(timm)^+$	CH_3OH	ca.240	IL	11
b	$Cu(TMP)_2^+$	CH_3OH	215 (23500)	IL	13
			239 (23100)	Cu → TMP CT	
c	$Cu(pza)^+$	CH_3OH	222 (20000)	IL	13
			254 (20600)	Cu → pza CT ($d\pi \rightarrow \pi_L^*$)	
			298 (2610)	Cu → pza CT ($d\sigma^* \rightarrow \pi_L^*$)	
d	$Cu(trpyn)^+$	CH_3OH	215 (17200)	IL	13
			261 (16500)	Cu → trpyn CT	
e	$Cu(dmp)_2^+$	CH_2Cl_2	454 (7950)	Cu → dmp CT	31
f	$Cu(bipy)(PPh_3)_2^+$	CH_3OH	355 (2820)	Cu → bipy CT	20
g	$Cu(phen)(PPh_3)_2^+$	CH_3OH	365	Cu → phen CT	25
h	$Cu(dmp)(PPh_3)_2^+$	CH_3OH	365 (2800)	Cu → dmp CT	25
i	$Cu(mbp)(PPh_3)_2^+$	CH_3OH	348 (2870)	Cu → mbp CT	20
j	$Cu(6,6'\text{-dmbp})(PPh_3)_2^+$	CH_3OH	340 (2850)	Cu → 6,6′-dmbp CT	20
k	$CuCl_3^{2-}$	1 M HCl, μ = 3 M	274 (4200)	CTTS	40
l	$Pb(N_3)_6^{2-}$	CH_3CN	318 (19500)	N_3 → Pb CT	46
m	$Sn(N_3)_6^{2-}$	CH_3CN	236 (14000)	N_3 → Sn CT	46
n	Zn(tdt)(phen)	$CHCl_3$	475 (80)	dith → phen CT	50
o	$[Au(dta)]_4$	CS_2	430 (1400)	$d \rightarrow s$	56
p	$Pd(PPh_3)_3$	2-MeTHF	~320 ($12\text{–}16\times10^3$)	$d \rightarrow p$	60
q	$Pt_2(dppm)_3$	2-MeTHF (77 K)	487 (27400)	$d \rightarrow p$	60
r	$Cu(PPh_3)_3Cl$	CH_2Cl_2/ cyclohexane	290–300	$\sigma \rightarrow a_\pi$	64
s	$Cu(prophos)BH_4$	Cyclohexane	300–320	$\sigma \rightarrow a_\pi$	62

π-antibonding orbital and results in the formation of a metal-to-ligand charge transfer excited state. A $\pi_L \rightarrow \pi_L^*$ transition occurs between two ligand-based orbitals and produces an intraligand excited state. A $d\sigma^* \rightarrow s\sigma^*$ transition results in a radial redistribution of electron density between orbitals localized on the metal and affords an interconfigurational metal-centered excited state. Representative examples of these and other transition types to be considered in this review are compiled in Table 1.

It should be noted that in some complexes a single molecular orbital configuration does not provide an adequate representation of the electronic distribution in a state and, as a result, interactions with one or more other configuration(s) must be considered. In the following discussion of the different types of electronic transitions in d^{10} systems, a few cases in which such configuration interaction plays a significant role will be treated.

(i) Intraligand transitions

Intraligand excited states of metal complexes arise from electronic transitions between orbitals localized primarily on a coordinated ligand (Fig. 1). Typically, the metal causes a relatively small (less than 1000 cm^{-1}) perturbation of the transition energy and this feature can be used as a diagnostic tool to aid in assignment [10]. A particularly straightforward example is provided by $Ag(timm)^+$ (Table 1, entry a), where timm is an imidazole-containing tridentate ligand (**I**) [11]. Figure 2 illustrates that the absorption spectrum of this complex possesses a broad band at about 240 nm which closely matches

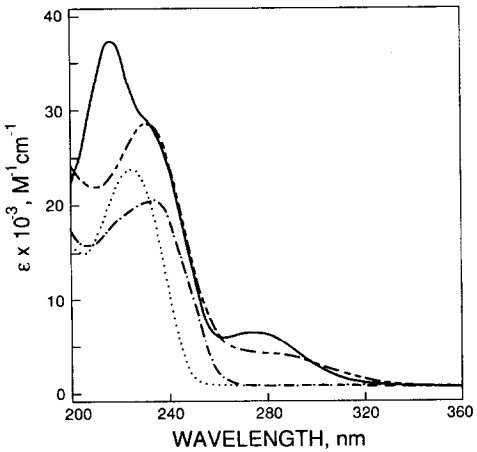

Fig. 2. Electronic absorption spectra in methanol of timm (· · · · · ·), $[Cu(timm)]BF_4$ (— - - —), $[Cu(timm)(CO)]BF_4$ (———) and $[Ag(timm)]BF_4$ (· – · – ·). Reprinted with permission from ref. 11. Copyright 1986 American Chemical Society.

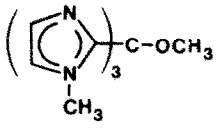

I

in energy and intensity the π–π^* transition of free imidazole. Such correspondence strongly supports the assignment of the band in question as an intraligand π_L–π_L^* transition. Likewise, bands appearing near 220 nm in the absorption spectra of two-, three- and four-coordinate pyrazole complexes (**II**–**IV**) are readily identified as intraligand π_L–π_L^* in character on the basis of their energetic similarity to transitions observed in the corresponding free pyrazole ligands (Table 1, entries b, c, d) [12,13].

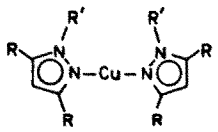

II

R = H,CH_3

R' = H,CH_3,C_2H_5

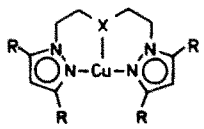

III

X = NH,O,S

R = CH_3,t-C_4H_9

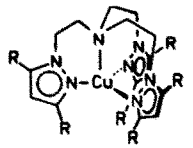

IV

R = H,CH_3,t-C_4H_9

The intense Q and Soret absorption bands of d^{10} metalloporphyrins are attributed to π_L–π_L^* transitions localized on the 16-membered porphyrin ring [14]. Both π_L–π_L^* and n–π^* (n refers to non-bonding electrons on the bridge nitrogen atoms) intraligand transitions occur in the related phthalocyanine complexes [14]. Bis(dithiolene) complexes of general formula $M[S_2C_2(CN)_2]_2^{2-}$ (M = Zn(II), Cd(II) or Hg(II)) display intense absorption bands of π_L–π_L^* character near 270 and 380 nm [15,16]. Intraligand π_L–π_L^* transitions are also evident in the high energy region of the spectra of $Cu(phen)(PPh_3)_2^+$ (see **V**) and related polypyridine complexes [17].

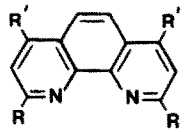

V

phen (R = H)

dmp (R = Me)

dpp (R = Ph)

tpp (R = R' = Ph)

Luminescence originating from an intraligand π_L–π_L^* excited state usually resembles that of the corresponding free ligand both with regard to energy and band structure. In contrast, the lifetime and/or the quantum yield of emission can differ substantially between the coordinated and free ligand. The behavior of $Zn(Ph_3CS)_2(phen)$ nicely exemplifies these points [18]. Illumination of the complex in an organic glass at 77 K causes the ap-

pearance of fluorescence and phosphorescence. Both bands are highly structured and closely mimick the known spectral characteristics of uncoordinated phen, although slight shifts in band energies and a lengthening of the phosphorescence lifetime result from coordination. Relative to free phen, there is also a noticeable increase in the fluorescence-to-phosphorescence intensity ratio. These two bands can be confidently assigned as intraligand emissions originating from the lowest $^1(\pi_L-\pi_L^*)$ and $^3(\pi_L-\pi_L^*)$ excited states of coordinated phen. Porphyrin complexes of closed-shell d^{10} metals such as zinc(II), cadmium(II) and tin(IV) typically undergo prompt fluorescence in room temperature fluid solution from an intraligand $\pi_L-\pi_L^*$ excited state [14]. In low temperature rigid media, $\pi_L-\pi_L^*$ phosphorescence can be detected. Intraligand $\pi_L-\pi_L^*$ fluorescence and phosphorescence from dithiolene complexes of zinc(II), cadmium(II) and mercury(II) has been observed [15,16].

Several complexes display intraligand emission as one component of a dual luminescence, the second component being charge transfer or $\sigma-a_\pi$ in character. Discussion of these interesting systems will be deferred until the other transition types are considered.

(ii) Metal-to-ligand charge transfer transitions

Metal-to-ligand charge transfer (MLCT) transitions occur with an outward flow of electron density from a metal-centered orbital to a predominantly ligand-based orbital (Fig. 1). Such transitions tend to be prominent in systems composed of an easily oxidized metal and a ligand containing a low energy acceptor orbital. Copper(I) complexes containing polypyridine ligands, for example, absorb strongly in the visible and near-UV regions owing to the presence of one or more band(s) of MLCT character (Table 1, entries e–j) [17,19–22]. Figure 3 depicts a qualitative energy level diagram for $Cu(phen)(PPh_3)_2^+$ in idealized C_{2v} symmetry. The phen ligand contains two low lying π^* orbitals which can accept electron density from the metal. Most of the charge transfer absorption intensity derives from transitions (indicated with arrows in Fig. 3) polarized along the C_2 axis of the complex.

Within the series $Cu(bipy)(PPh_3)_2^+$, $Cu(mbp)(PPh_3)_2^+$ and $Cu(6,6'\text{-dmbp})(PPh_3)_2^+$ (see **VI**) the charge transfer absorption maximum shifts progressively toward higher energy upon introduction of electron-donating methyl groups (Table 1, entries f, i, j) [20]. While several factors may contribute to this behavior, it should be noted that the half-wave potentials of aromatic systems generally shift cathodically upon methylation. Since the MLCT transition can be viewed, in a formal sense, as an oxidation of the metal center accompanied by reduction of the polypyridine ligand, the blue

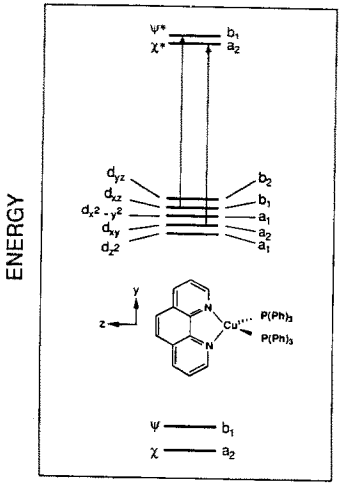

Fig. 3. Energy level diagram and axis system for Cu(phen)$(PPh_3)_2^+$. Arrows indicate *z*-polarized MLCT transitions in C_{2v} symmetry. Labels ψ and χ designate molecular orbitals composed primarily of ligand-based π orbitals which are antisymmetric and symmetric respectively with respect to rotation about the twofold axis; asterisks denote empty orbitals. Reprinted with permission from ref. 17. Copyright 1987 American Chemical Society.

shift of the absorption band correlates well with simple predictions based upon ligand electron-acceptor properties.

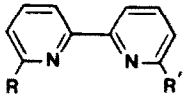

bipy (R = R' = H)
mbp (R = H, R' = Me)
6,6'-dmbp (R = R' = Me)

VI

Cu(I)–polypyridine complexes display a notable propensity to luminesce, and this property can be exploited to obtain important information about excited state energetics and dynamics in these systems [17,19–30]. The emission characteristics of a series of Cu(5-X-phen)$(PPh_3)_2^+$ complexes measured in a low temperature glassy matrix are summarized in Table 2. The spectrum of each compound can be time resolved into two separate and non-equilibrated components; a long-lived (ms) emission exhibiting well-defined vibronic structure and a short-lived (μs) structureless emission occurring at somewhat lower energy. The structured component can be assigned straightforwardly as intraligand phosphorescence from a $^3(\pi_L-\pi_L^*)$ state of coordinated 5-X-phen on the basis of its similarity in energy and bandshape to the $\pi-\pi^*$ phosphorescence of the free ligand. Reasonable arguments have been presented that the unstructured component of the emission be assigned as a phosphorescence from an MLCT triplet state [17].

TABLE 2

Luminescence data [17] for Cu(5-X-phen)$(PPh_3)_2^+$ complexes [a]

X	$^3(\pi_L-\pi_L^*)$ emission		^{3}MLCT emission		ΔE (cm^{-1})
	λ_{max} (nm)	τ (ms)	λ_{max} (nm)	τ (μs)	
H	461				
	497	8.5	600	103	600
	528				
CH_3	473				
	504	10.5	588	85	400
	536				
Cl	483				
	514	14.5	590	75	0
	550				
Ph	506 (sh)	34.5	599	71	−1000
	560				

[a] Spectra measured at 77 K in ethanol–methanol (4:1 v/v); excitation wavelength is 385 nm.

The key to understanding the dual emissions in these systems is to recognize that ^{3}MLCT and $^3(\pi_L-\pi_L^*)$ possess very different equilibrium geometries [17,25,29]. Thus the ^{3}MLCT state, which formally contains a d^9 Cu(II) center subject to the pseudo-Jahn–Teller effect, should be considerably distorted from the ground state geometry of the complex. In contrast, the intraligand $^3(\pi_L-\pi_L^*)$ state retains a d^{10} Cu(I) center and little change in geometry is expected. Since structural changes should be inhibited at low temperatures in a rigid matrix, the interconversion between the two states is slow relative to competing decay processes. Figure 4 depicts this basic idea in terms of potential energy surfaces. The excited states are assumed to undergo vibronic mixing along a generalized nuclear displacement coordinate, Q_0, which describes the reorganization of the solvent media and any structural changes within the complex. In essence, Q_0 defines the "reaction coordinate" for internal conversion between $^3(\pi_L-\pi_L^*)$ and ^{3}MLCT. When the barrier height along Q_0 is large relative to the available thermal energy, conversion is hindered, and dual non-equilibrated emissions result.

It has been noted that internal conversion from $^3(\pi_L-\pi_L^*)$ to ^{3}MLCT can be regarded as an intramolecular electron transfer process involving the exchange of an electron between a copper $3d$ orbital and a π orbital of the polypyridine ligand [17,25]. As such, the conversion rate can be analyzed in terms of Marcus theory. While this theory predicts that several factors can affect the rate, one particularly important parameter is the driving force which, as seen in Fig. 4, can be equated to the difference in the zero–zero

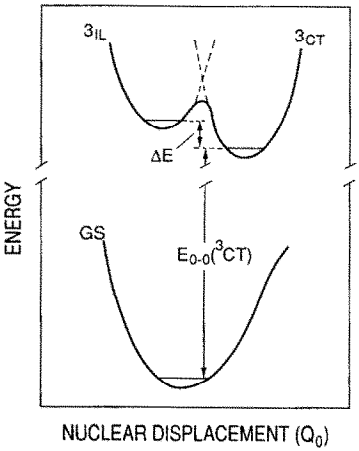

Fig. 4. Potential energy surfaces for the ground state (GS) and lowest energy excited states of a Cu(5-X-phen)$(PPh_3)_2^+$ complex. The broken lines indicate zero-order intraligand (IL) and metal-to-ligand charge transfer (CT) surfaces. The zero–zero energy (E_{0-0}) of the ^{3}CT state and the difference between the zero–zero energies (ΔE) of the ^{3}IL and ^{3}CT states also are indicated. Reprinted with permission from ref. 17. Copyright 1987 American Chemical Society.

energies of the two excited states, ΔE. For small ΔE values, the rate of electron transfer (internal conversion) is expected to increase with the driving force. In support of this prediction, the lifetime of the $^3(\pi_L-\pi_L^*)$ state decreases as the driving force for conversion to the ^{3}MLCT state becomes more favorable (ΔE increases in Table 2).

Luminescence intensities of Cu(I)–polypyridine complexes in fluid media can vary greatly, depending upon the nature of the solution environment. Thus the MLCT emission exhibited by $Cu(dmp)_2^+$ (see **V**) in a weakly basic solvent such as chloroform is completely quenched in coordinating solvents such as acetonitrile, methanol and water [31]. Moreover, the emission can be quenched by coordinating anions such as NO_3^-, ClO_4^- and BF_4^- [32]. This interesting quenching behavior has been ascribed to the formation of an exciplex (excited state complex) between the MLCT excited state of $Cu(dmp)_2^+$ and the quencher [33,34]. Figure 5 depicts this process in terms of potential energy surfaces that describe the approach of the quencher to the copper complex in its ground (lower curve) and excited (upper curve) states. Along the ground state surface, the tetracoordinate d^{10} Cu(I) center has little affinity for another ligand and close approach of the quencher causes a repulsive interaction. In contrast, the metal in the MLCT state formally exists as d^9 Cu(II), a coordinatively unsaturated species that can enhance its stability by the addition of a fifth ligand. Consequently, the excited state surface contains a minimum that corresponds to the five-coor-

dinate exciplex. Several mechanisms by which exciplex formation may facilitate radiationless decay to the ground state have been suggested [34]. (1) The decreased energy gap between the two surfaces at the configuration of the exciplex can result in more favorable Franck–Condon factors associated with crossing to the ground state surface. (2) The close approach of the two surfaces may lead to a mixing of states that enhances crossing to the ground state. (3) Coordination of a fifth ligand may cause a reordering of the excited state manifold such that an intrinsically shorter-lived state falls below the emissive MLCT state and mediates decay.

While attempts at direct observation of exciplex formation between the MLCT state of a copper(I) complex and a quencher have been unsuccessful to date, compelling evidence exists for the associative nature of quenching in these systems. For example, while a few percent of methanol almost totally quenches the emission from $Cu(dmp)_2^+$ in dichloromethane, the phenyl-substituted analogue $Cu(dpp)_2^+$ (see **V**) luminesces in pure methanol [21]. The simplest explanation for this disparity between the two complexes is that the bulky phenyl groups on dpp effectively shield the metal from associative attack by the alcohol. Similarly, within the series $Cu(bipy)(PPh_3)_2^+$, $Cu(mbp)(PPh_3)_2^+$ and $Cu(6,6'\text{-dmbp})(PPh_3)_2^+$ (see **VI**), the relative luminescence increases upon introduction of methyl groups in positions adjacent to the donor nitrogen atoms of the bipyridine ligand [20]. Here again, the substituents block access to the metal and thereby prevent coordination of a quencher molecule.

Excited state absorption and resonance Raman spectroscopies have been employed recently to probe the electronic structures of the MLCT states of

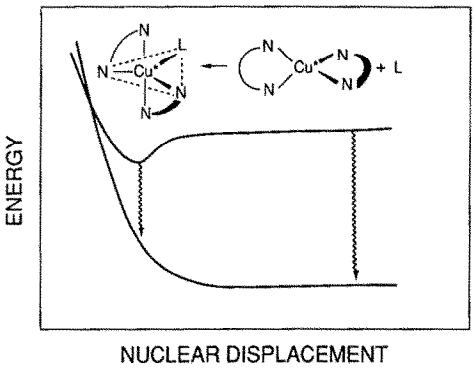

Fig. 5. Schematic energy surfaces for exciplex quenching of the MLCT excited state of a copper(I) complex by quencher L. Upper surface depicts the approach of L to the photoexcited complex to form a stabilized exciplex represented by the minimum. The latter species then decays to the lower ground state surface. Reprinted with permission from ref. 34. Copyright 1987 American Chemical Society.

Cu(I)–polypyridine complexes [35–37]. Figure 6 displays the absorption spectrum of the Cu → dpp charge transfer excited state in $Cu(dpp)_2^+$. By selective irradiation into different regions of the spectrum, it is possible to observe resonantly-enhanced Raman features characteristic of either the neutral dpp ligand (360 nm excitation) or the dpp^- radical anion (540 nm excitation). This finding strongly supports a localized formulation of the MLCT state, $(dpp)Cu^{II}(dpp^-)^+$, in which the transfer electron resides on a single polypyridine ligand [36].

While polypyridines have emerged as the most popular class of ligands in studies of MLCT behavior in d^{10} systems, some other ligand types deserve to be mentioned. The ligand timm (**I**), for example, forms several complexes containing prominent MLCT transitions (Fig. 2) [11]. The bands at 232 and 285 nm in the absorption spectrum of $Cu(timm)^+$ correspond to $d\pi-\pi_L^*$ and $d\sigma^*-\pi_L^*$ transitions (see Fig. 1) respectively, and as expected, substitution of copper(I) by the less-reducing silver(I) shifts both transitions to higher energy. Binding of carbon monoxide to $Cu(timm)^+$ to form the four-coordinate adduct also moves the MLCT band to higher energy with the $d\pi-\pi_L^*$ band being affected to a greater extent (Fig. 2). This latter result reflects the greater stabilization of the metal $d\pi$ orbitals caused by π backbonding to the coordinated CO. In an alcohol glass at 77 K, $Cu(timm)^+$ displays a broad structureless MLCT luminescence with a maximum at 592 nm. Consistent with the absorption spectral behavior, addition of CO causes a blue shift of the emission to 550 nm. Interestingly, this 550 nm band in $Cu(timm)(CO)^+$ closely mimicks the luminescence observed for the carbonyl

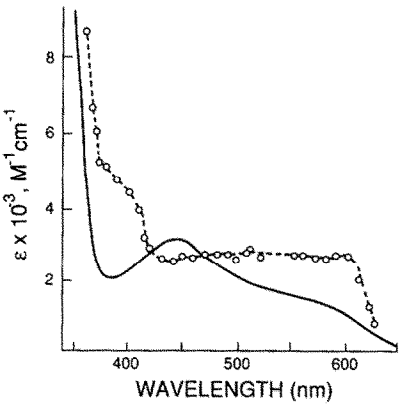

Fig. 6. Excited state (O---O) and ground state (———) absorption spectra of $Cu(dpp)_2^+$ in $CHCl_3$. The broad band in the excited state spectrum arises from a radical-centered (dpp^-) $\pi-\pi^*$ transition, while absorption in the 360 nm region is ascribed to an LMCT (dpp → Cu(II)) transition. Reprinted with permission from ref. 35. Copyright 1986 Elsevier Science Publishers.

form of hemoglobin, a result which suggests that the copper sites in this protein are ligated by three imidazole groups.

Intense MLCT transitions have also been observed in the UV spectra of an extensive series of copper(I) complexes containing pyrazole derivatives (**II–IV**) [12,13]. Changes in the coordination environment strongly influence the transition energies (Table 1, entries b, c, d). Thus the transition decreases in energy in changing from two- to four-coordination, most probably as the result of increasing electron density at the metal center. Moreover, the largest splitting between the $d\pi$ and $d\sigma^*$ orbitals occurs in the three-coordinate complexes, thereby accounting for the observation that only in these systems are the $d\pi$–π_L^* and $d\sigma^*$–π_L^* transitions clearly resolved. All the complexes exhibit MLCT luminescence at 77 K in an ethanol glass, and in many cases the luminescence persists at room temperature in a weakly coordinating solvent.

Each of the metal atoms in the binuclear $M_2(dba)_3$ and trinuclear $M_3(tbaa)_3$ complexes (where M = Pd(0) or Pt(0), dba = **VII**, and tbaa =

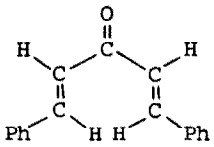

VII

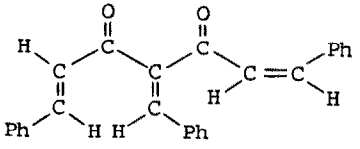

VIII

VIII) is trigonally coordinated to an olefinic group contained in each of three bridging ligands. The intense purplish color of these complexes arises from an absorption band which has been assigned as predominantly MLCT in character [38]. All the compounds exhibit relatively strong MLCT phosphorescence following photoexcitation in fluid solution at room temperature. Interestingly, luminescence also occurs when a working electrode, immersed in a low temperature solution of either Pt(0) complex, is pulsed between cathodic and anodic potentials sufficient to generate the reduced (P^-) and oxidized (P^+) forms of the parent compounds. This electrogenerated chemiluminescence (ECL) results from a radical cation–anion annihilation process

$$P^- + P^+ \longrightarrow P + P^* \qquad (1)$$

which, in these systems, is sufficiently exoergic for one of the neutral molecules to be regenerated in its luminescent excited state (P^*). Consistent with this mechanism, the ECL spectra of $Pt_2(dba)_3$ and $Pt_3(tbaa)_3$ closely match the corresponding photoluminescence spectra [38].

(iii) Charge-transfer-to-solvent transitions

In the absence of a low energy ligand acceptor orbital, a d^{10} complex may undergo a transition involving the radial displacement of an electron into the surrounding solvent. This charge-transfer-to-solvent (CTTS) transition should be most common in anionic complexes where coulombic repulsion favors charge separation. Both $CuCl_3^{2-}$ (Table 1, entry k) [39–42] and $Cu(CN)_3^{2-}$ [43], for example, display a UV absorption band in aqueous media arising from a CTTS transition. This assignment follows from the characteristic wavelength shifts of this band upon changing the solvent composition and temperature and, most importantly, from the observation of photoelectron production in solution (vide infra). The last process also occurs for the cationic complex $Cu(NH_3)_3^+$, prompting the assignment of its UV absorption band(s) as CTTS in character [44].

Irradiation into the 274 nm CTTS absorption band of $CuCl_3^{2-}$ in room-temperature aqueous solution containing 5 M chloride ion results in luminescence centered at 470–480 nm [45]. The emission is quenched by protons but with a rate law different from that observed for scavenging of the photoejected electron. This key observation, the long radiative lifetime (greater than 30 μs, depending upon additives), and the large Stokes shift between the absorption and emission bands indicate that the luminescence does not originate from the CTTS singlet state populated in absorption, but instead comes from a lower energy spin-forbidden excited state. The suggestion has been made that the emissive state possesses metal-centered d–s orbital character (see Section B(vi)), although the alternative assignment of a CTTS triplet cannot be discounted [45]. Further studies of this interesting luminescence behavior are warranted.

(iv) Ligand-to-metal charge transfer transitions

Ligand-to-metal charge transfer (LMCT) transitions in d^{10} complexes result in the movement of electron density from a ligand-based orbital into a vacant s or p orbital on the metal, (i.e. $s\sigma^*$ or $p\sigma^*$ in Fig. 1). For a given ligand, the transition energy depends upon the electron-accepting ability of the metal. Thus LMCT transitions occur at lower energies in $Pb(N_3)_6^{2-}$ than in $Sn(N_3)_6^{2-}$ (Table 1, entries l and m) owing to the greater optical electronegativity of lead(IV) (1.9) relative to tin(IV) (1.5) [46]. Analogous reasoning accounts for the observation that Ag^+ dissolved in tetrahydrofuran displays an LMCT band (corresponding to transfer of a non-bonding electron on the oxygen atom of the ether to Ag^+) at 305 nm, whereas the less-oxidizing Cu^+ possesses no comparable feature above 280 nm [47]. Although a detailed spectral analysis is lacking, the presence of one or more

LMCT transitions in the absorption spectra of diarylcadmium(II) [48] and bis(cyclopentadienyl)mercury(II) [49] compounds can be inferred from the nature of their UV photochemical behavior (vide infra).

There have been no reports of luminescence from LMCT excited states of d^{10} complexes.

(v) Ligand-to-ligand charge transfer transitions

Colored complexes result when zinc(II) and cadmium(II) are coordinated to an N-heterocyclic bidentate ligand such as phen and either a bidentate aromatic dithiolate or two monodentate benzenethiolate ligands [18,50,51]. Absorption measurements reveal that the colors arise from a long-wavelength band which appears only when ligands of both types are present in the complex. Thus $ZnCl_2$(phen), which lacks a thiolate ligand, is a white solid. The long-wavelength band has been attributed to a ligand-to-ligand charge transfer (LLCT) transition in which electron density flows from the highest occupied molecular orbital of the thiolate ligand to the lowest unoccupied molecular orbital of the N-heterocycle through the metal ion. Figure 7 depicts this novel type of charge transfer process in schematic fashion. In general, both electron-donating substituents on the thiolate and electron-withdrawing groups on the N-heterocycle decrease the transition energy. Significant but smaller shifts in energy can be induced by changes in solvent. This flexibility allows the position of the LLCT band to be tuned over a wide portion of the visible region.

These mixed-ligand d^{10} complexes display some highly interesting luminescence properties in the solid state. Within the series Zn(4-X-PhS)$_2$(phen), for example, the type of luminescence observed depends upon both the identity of the X substituent and the temperature [52,53]. When X is Cl, the 6.5 K spectrum consists of two overlapping bands: a structured phosphorescence ($\tau = 0.39$ s) that originates from the lowest $^3(\pi_L - \pi_L^*)$

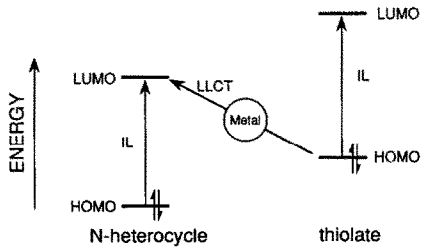

Fig. 7. Schematic representation of the lowest energy ligand-to-ligand charge transfer (LLCT) transition in a metal complex. HOMO and LUMO denote the highest occupied and lowest unoccupied molecular orbitals respectively, while IL refers to an intraligand transition.

excited state of coordinated phen and a more intense, broad phosphorescence ($\tau = 8$ ms) arising from the lowest ^{3}LLCT excited state (LLCT) fluorescence also is observed in time-resolved experiments). The different lifetimes indicate that the two emissive triplets are not in thermal equilibrium. Sharply contrasting behavior occurs when X is Me in that intraligand phosphorescence from phen now dominates the emission spectrum. Finally, when X is OMe, only LLCT phosphorescence is observed.

Significantly, the two orbitally-distinct emissions possess different temperature dependences [52,53]. Raising the temperature causes a decrease in the intensity of intraligand phosphorescence and a concomitant increase in the intensity of LLCT phosphorescence. Thermally modulated emission measurements provide unequivocal evidence that this behavior reflects a thermally activated redistribution of electronic energy from the $^3(\pi_L{-}\pi_L^*)$ state to the ^{3}LLCT state. A highly simplified treatment of this process is presented in Fig. 8 (see ref. 53 for a more detailed analysis), where ΔE represents the energy gap between the two excited states and E^* denotes the activation barrier for energy transfer. When X is Cl or Me, estimates place ΔE at less than 1500 cm^{-1} and E^* at about 140 cm^{-1}. The latter value is sufficiently large to ensure that essentially no communication occurs between $^3(\pi_L{-}\pi_L^*)$ and ^{3}LLCT at 6.5 K and thus distinct emission arises from each of these states following broad-band photoexcitation. At higher temperatures, thermally activated transfer to ^{3}LLCT becomes significant and phosphorescence characteristic of this latter state increases in importance. However, when X is OMe, ΔE appears to be substantially greater than 1500

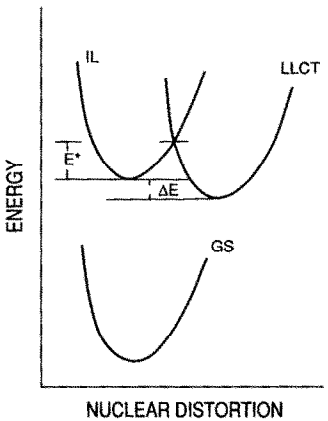

Fig. 8. Potential energy surfaces for Zn(4-X-PhS)$_2$(phen) complexes. GS denotes the ground state, whereas IL and LLCT represent intraligand and ligand-to-ligand charge transfer excited states respectively. Also shown are the energy gap between the two excited states (ΔE) and the activation barrier for energy transfer between states (E^*).

cm^{-1} while E^* has dropped to a value where efficient crossing from $^3(\pi_L-\pi_L^*)$ to ^{3}LLCT occurs even at 6.5 K. Thus only LLCT phosphorescence is observed for this complex. Additional studies are required to determine whether the apparent correlation between the activation energy (E^*) and the driving force (ΔE) for energy transfer is generally valid. Nonetheless, the results to date support earlier contentions that slow energy transfer between excited states is favored when (a) the states are derived from configurations of different orbital parentage, and (b) the states are of similar energy.

(vi) Interconfigurational metal-centered transitions

Two types of interconfigurational metal-centered transitions have been identified in d^{10} systems. The first, characterized by an $(n-1)d^{10} \rightarrow (n-1)d^9ns^1$ orbital change (n denotes principal quantum number), is parity forbidden and thus of low intensity. Consequently, $d \rightarrow s$ transitions are easily hidden under more intense charge transfer and intraligand absorption bands. This problem is minimized in Cu^+-doped NaF crystals, since the d^{10} ion resides in an octahedral environment of F^- ions that resist redox processes and possess no low energy internal transitions. Under these circumstances, charge transfer and intraligand bands lie at very high energies and well-resolved singlet $3d \rightarrow 4s$ transitions can be observed in the absorption spectrum around 300 nm [54]. The low temperature luminescence spectrum of Cu^+-doped $RbMgF_3$ crystals displays bands at 450 and 575 nm. These features have been assigned as interconfigurational $4s \rightarrow 3d$ phosphorescence arising from Cu^+ situated in two different lattice sites [55].

Low energy $5d \rightarrow 6s$ transitions appear in the absorption spectra of the tetranuclear clusters $[Au(dta)]_4$ (Table 1, entry o) and $[Au(pip)Cl]_4$ [56]. Both complexes adopt the basic structure shown in **IX** and the short Au–Au

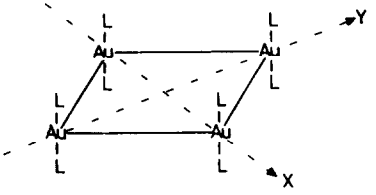

IX

distances suggest the existence of metal–metal bonding. Figure 9 contains a simplified molecular orbital model of the bonding within the square-planar (D_{4h}) Au_4 core. Each gold atom employs one d and one s orbital in σ bonding to its closest neighbors. In the simplest case (no configuration interaction), the lowest bonding (b_{2g}), non-bonding (e_u), and antibonding (a_{2g}) molecular orbitals composed largely of the $5d$ metal orbitals are

completely filled and no net metal–metal bonding occurs. Mixing of the $5d$ and $6s$ orbitals, however, results in a stabilization of the occupied e_u orbital and enhanced stability of the cluster. The lowest energy singlet and triplet excited states in the cluster arise from the $a_{2g} \rightarrow a_{1g}$ (mainly $d \rightarrow s$) orbital transition. Since this transition results in the promotion of an electron from an antibonding to a bonding orbital, the overall bond order within the Au_4 core should increase with a concomitant decrease in Au–Au distance. Evidence for this excited state bond contraction is provided by low temperature luminescence spectroscopy. Each cluster shows a broad unstructured phosphorescence arising from a spin-forbidden $a_{1g} \rightarrow a_{2g}$ orbital transition (Fig. 9), and the large Stokes shift of this band has been attributed, at least in part, to structural differences between the excited and ground states. Photoinduced bond shortening also accounts for the Stokes-shifted $4s \rightarrow 3d$ phosphorescence emanating from the cubane-like tetranuclear clusters $[Cu(py)I]_4$ and $[Cu(pip)I]_4$ [57].

The second type of interconfigurational metal-centered transition involves a parity-allowed $(n-1)d^{10} \rightarrow (n-1)d^9np^1$ orbital change. Several recent studies report the observation of low energy $d \rightarrow p$ transitions in mononuclear and binuclear complexes of nickel(0), palladium(0) and platinum(0) containing phosphine, phosphite or arsine ligands [58–60]. Figure 10 displays a simple molecular orbital energy level diagram for d^{10} ML_3 and d^{10}–d^{10} $(ML_3)_2$ complexes. In ML_3 systems with D_{3h} symmetry, the singlet $(d_{xy}, d_{x^2-y^2}) \rightarrow p_z$ transition lies lowest in energy but is orbitally forbidden. The higher lying $d_{z^2} \rightarrow p_z$ and $(d_{xz}, d_{yz}) \rightarrow p_z$ singlet transitions are allowed, however, and one or both presumably are responsible for the strong band at

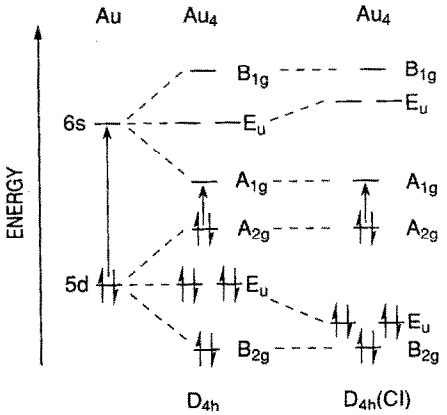

Fig. 9. Qualitative molecular orbital diagram of the bonding within the square-planar Au_4 cores of $[Au(dta)]_4$ and $[Au(pip)Cl]_4$. Two cases are depicted: D_{4h} (no configuration interaction) and D_{4h} (CI) (configuration interaction included). Reprinted with permission from ref. 56. Copyright 1988 Elsevier Science Publishers.

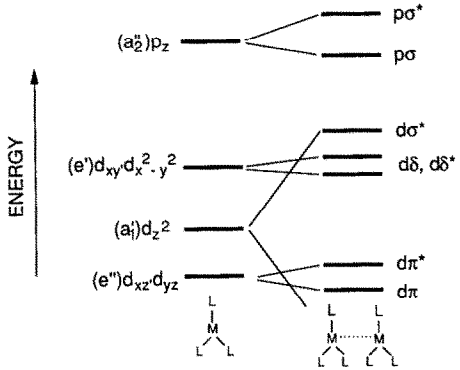

Fig. 10. Molecular orbital diagram for d^{10} ML_3 and d^{10}–d^{10} $(ML_3)_2$ complexes. Reprinted with permission from ref. 60. Copyright 1988 American Chemical Society.

about 320–330 nm in the absorption spectra of $Pd(PPh_3)_3$ and $Pt(PPh_3)_3$. In binuclear $(ML_3)_2$ complexes the two sets of orbitals on contiguous metal atoms interact and split as shown in Fig. 10. The intense absorption between 400–500 nm in the spectra of $Pd_2(dppm)_3$ and $Pt_2(dppm)_3$ has been attributed to a singlet $d\sigma^* \rightarrow p\sigma$ transition [60].

These zerovalent d^{10} complexes typically display a broad visible phosphorescence both in low temperature matrices and room temperature fluid solution. Selected lifetime data obtained under each set of conditions are compiled in Table 3. For $Pd(PPh_3)_3$ and $Pt(PPh_3)_3$ the emission arises from a spin-forbidden $p_z \rightarrow (d_{x^2-y^2}, d_{xy})$ orbital transition, whereas the spin-forbidden $p\sigma \rightarrow d\sigma^*$ transition is responsible for phosphorescence from the binuclear complexes [60].

(vii) σ–a_π *transitions*

Arylphosphine molecules such as PPh_3 and diphos exhibit an intense UV absorption band arising from an l–a_π transition [61,62] (see ref. 63 for an

TABLE 3

Phosphorescence data [60] for zerovalent metal–phosphine complexes [a]

Complex	295 K		77 K	
	τ (μs)	λ_{max} (nm)	τ (μs)	λ_{max} (nm)
$Pd(PPh_3)_3$	6.61	635	98	590
$Pd_2(dppm)_3$	5.93	710	107	685
$Pt(PPh_3)_3$	0.69	705	24.9	645
$Pt_2(dppm)_3$	< 0.02	790	10.6	790

[a] Measured in 2-methyltetrahydrofuran.

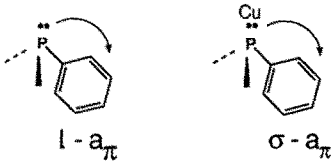

Fig. 11. Pictorial representation of the $l-a_\pi$ transition in arylphosphine molecules and the $\sigma-a_\pi$ transition in Cu(I)–arylphosphine complexes.

alternative assignment). This type of transition involves the promotion of an electron from the lone pair orbital (l) on phosphorus to an empty antibonding orbital of π origin (a_π) situated on a phenyl ring (Fig. 11). Upon coordination of the phosphine molecule, the electron pair that formerly resided in the l orbital now engages in σ bonding to the metal atom. Accordingly, the transfer of an electron from this σ orbital to the a_π orbital of the phenyl ring has been designated as a $\sigma-a_\pi$ transition (Fig. 11) [61,62]. Since the π system of the phosphine ligand may interact with metal d-orbitals of appropriate symmetry, a mechanism exists for delocalization of π-electron density over the entire metal–phosphine unit during a $\sigma-a_\pi$ transition [64]. While the net effect of the excitation process could be considered as a type of metal-to-ligand charge transfer, we prefer the more specific $\sigma-a_\pi$ designation.

Spectroscopic studies of (arylphosphine)copper(I) tetrahydroborate complexes and of the corresponding uncoordinated phosphine molecules have provided some interesting insights into the properties of $\sigma-a_\pi$ transitions. A comparison of PPh_3 and $Cu(PPh_3)_2BH_4$ (**X**), for example, reveals that the change in the orbital nature of the most intense absorption band from $l-a_\pi$ to $\sigma-a_\pi$ causes a relatively minor perturbation in transition energy and bandshape (Fig. 12) [61,65]. At first glance this result seems surprising, since transitions involving lone pair electrons generally shift to considerably higher energy upon protonation or complexation of the lone pair. That this shift does not occur for the singlet $\sigma-a_\pi$ transition of $Cu(PPh_3)_2BH_4$ suggests that metal–phosphorus π-backbonding plays a role in determining the transition energy (the modified $\sigma,d-a_\pi$ nomenclature has been suggested to emphasize such d orbital participation) [64]. In comparing diphos and $Cu(diphos)BH_4$ (**XI**), we encounter distinctly different spectral behavior

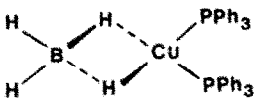

X

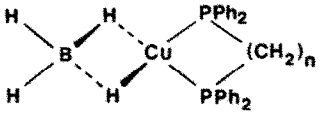

XI (n = 2)
XII (n = 3)

from that just described. Thus two transitions which appear to be singlet $\sigma-a_\pi$ in character occur at appreciably lower energies than the $l-a_\pi$ transition in free diphos (Fig. 12) [61,65]. A possible explanation for this behavior is provided by the observation that the energy of the $l-a_\pi$ transition in arylphosphines drops upon the introduction of alkyl groups at the *ortho* positions of the aromatic ring [66–68]. It is thought that steric crowding by these substituents alters the C–P–C valence angle and/or the twist angle (angle between the axis of the phosphorus *l*-orbital and the axis of the adjacent carbon $2p\pi$-orbital) from the characteristic value(s) in the uncoordinated phosphine and thereby affects the transition energy. In a similar fashion, steric constraints imposed by formation of the five-membered chelate ring in Cu(diphos)BH_4 may cause changes in one or both angles with an accompanying lowering of the transition energy. Furthermore, the splitting observed in the spectrum of Cu(diphos)BH_4 suggests that the equivalence of the two phenyl groups attached to each phosphorus atom in diphos has been destroyed by coordination to the metal. Consequently, transitions to the a_π orbitals of each aromatic ring can occur with different energies [61].

Luminescence lifetime data for several (arylphosphine)copper(I) complexes are summarized in Table 4. In room-temperature fluid solution, Cu(diphos)BH_4 and Cu(prophos)BH_4 (**XII**) each exhibits a broad microsecond phosphorescence that originates from the lowest $^3(\sigma-a_\pi)$ excited state [62]. Under comparable experimental conditions, however, neither

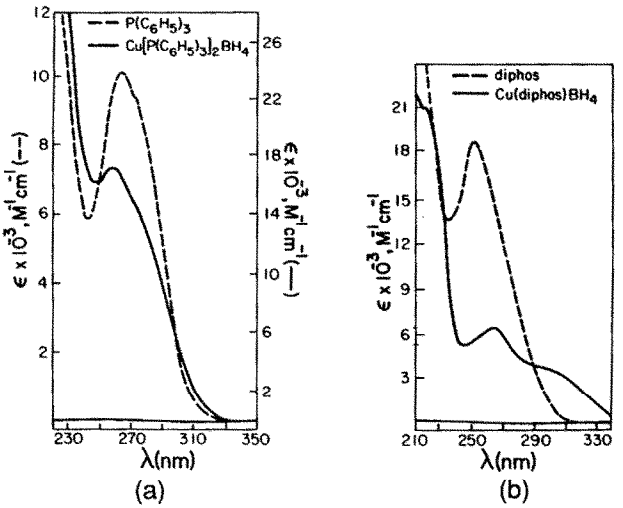

Fig. 12. Electronic absorption spectra of (a) PPh_3 and $Cu(PPh_3)_2BH_4$, and (b) diphos and Cu(diphos)BH_4 in cyclohexane at room temperature. Reprinted with permission from ref. 65. Copyright 1977 American Chemical Society.

TABLE 4

Phosphorescence lifetimes of selected (arylphosphine)copper(I) complexes [62,64,69]

Complex	τ	
	77 K	Room temperature [a]
$Cu(PPh_2Me)_3Cl$	4 ms [b]	No phosphorescence
$Cu(PPh_3)_2BH_4$	2.1 ms [c]	No phosphorescence [d]
	0.8 ms	
Cu(diphos)BH_4	– [e]	1.1 μs
Cu(prophos)BH_4	0.7 ms	3.9 μs

[a] Measured in benzene solution. [b] Measured in EPA glass. [c] Measured in toluene glass. [d] Fluorescence ($\tau < 10$ ns) observed. [e] Not measured.

$Cu(PPh_2Me)_3Cl$ nor $Cu(PPh_3)_2BH_4$ phosphoresces even though intersystem crossing to $^3(\sigma\text{–}a_\pi)$ is highly efficient in these complexes [62,64]. While no compelling explanation for this disparity in phosphorescence yields exists at present, it has been suggested that the triplet states of the chelated phosphine complexes may possess larger radiative rate constants than their non-chelated counterparts owing to differences in the twist angle about the P–phenyl bond [62].

Some interesting contrasts between the low temperature luminescence properties of the complexes in Table 4 also deserve note. Thus at 77 K, both $Cu(PPh_2Me)_3Cl$ in EPA glass and Cu(prophos)BH_4 in several different glassy matrices exhibit a single phosphorescence from the lowest $^3(\sigma\text{–}a_\pi)$ excited state [64,69]. The emission spectrum of $Cu(PPh_3)_2BH_4$, however, contains either one or two bands, depending upon the nature of the solvent matrix (Fig. 13) [69]. For the dual luminescence case, the dependence of the overall bandshape on excitation wavelength and the variation of lifetime

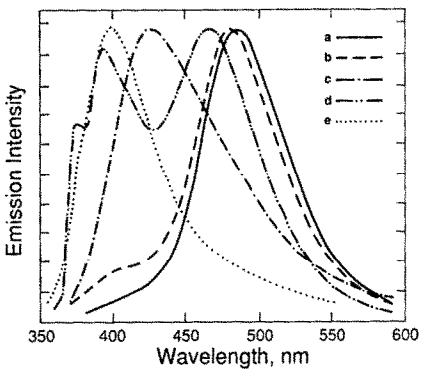

Fig. 13. Low temperature (77 K) emission spectra of $Cu(PPh_3)_2BH_4$ in (a) cyclohexane, (b) benzene, (c) chloroform, (d) EPA glass, and (e) toluene–chloroform (1:1 v/v). Reprinted with permission from ref. 69. Copyright 1984 American Chemical Society.

across the emission spectrum indicate that the two bands arise from different thermally non-equilibrated excited states. The higher energy band (τ = 2.1 ms) resembles the π–π^* phosphorescence of protonated PPh_3, and accordingly it has been assigned as intraligand phosphorescence from the $^3(\pi_L$–$\pi_L^*)$ state of the coordinated phosphine. The lower energy emission ($\tau = 0.8$ ms) also is a phosphorescence and originates from the $^3(\sigma$–$a_\pi)$ excited state. Given the diversity of the luminescence observed in different matrices (σ–a_π emission only, π_L–π_L^* emission only, dual emissions; see Fig. 13), it is evident that the solvent strongly influences the energetics and dynamics of these excited states. Factors such as a solvent-dependent energy gap between $^3(\sigma$–$a_\pi)$ and $^3(\pi_L$–$\pi_L^*)$ and solvent-assisted geometry changes have been suggested as contributing to this intriguing behavior [69].

(viii) Luminescence thermochromism in d^{10} *complexes*

Several copper(I) complexes of stoichiometry $Cu(N)_mX$, where N is a cyclic nitrogen base, X is Cl^-, Br^- or I^-, and $m = 1$–3, display visible luminescence when excited in the solid state [70,73]. In some cases the color of the emission undergoes a reversible change with temperature. Spectroscopic studies of this phenomenon, aptly termed luminescence thermochromism, indicate that it results from the presence of two (or more) emissive excited states, the relative populations of which vary with temperature. Thus at room temperature, $[Cu(py)I]_4$ undergoes only interconfigurational metal-centered (d–s) emission at 560 nm (see Section B(vi)), whereas at low temperature this band shifts to 610 nm and a second band, characterized as MLCT (Cu → py) emission, appears at 440 nm [71,72]. To the naked eye, this new distribution of emission wavelengths appears as a visible color change.

Another more subtle temperature effect that can contribute to luminescence thermochromism in solids involves temperature-induced structural changes. Consider the complex $Cu_4I_4(quin)_4$, in which the quinoline ligands (one per copper atom) project from the Cu_4I_4 framework in close (3.30 Å) and parallel planes. At room temperature the solid exhibits a broad featureless MLCT (Cu → quin) luminescence at 625 nm (Fig. 14). Upon cooling to 15 K, however, considerable fine structure characteristic of intraligand emission from quinoline develops on the high energy side of this broad band. It has been proposed that lowering the temperature decreases the distance between proximate quinoline ligands in the crystal to the point where an intermolecular interaction between the π systems enhances the probability of $(\pi_L$–$\pi_L^*)$ luminescence [73]. While the nature of this interaction was not specified, it was noted that crystalline $Cu_2I_2(quin)_4$, which is devoid of close quinoline–quinoline contacts, displays no intraligand emission at low temperature.

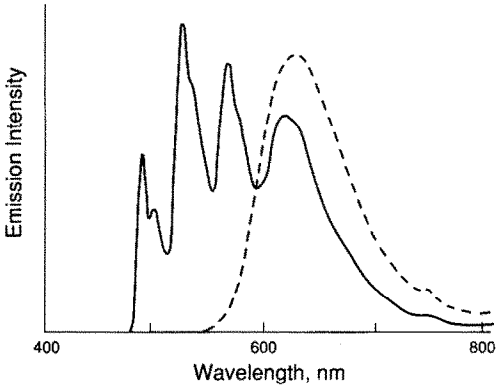

Fig. 14. Emission spectra of $Cu_4I_4(quin)_4$ at 15 K (———) and 235.5 K (— — —). Reprinted with permission from ref. 73. Copyright 1986 Royal Society of Chemistry.

C. PHOTOCHEMICAL PROPERTIES

Electronic spectroscopy has provided important information about the orbital parentages, energies, structures and lifetimes of the excited states present in d^{10} metal complexes. This information, in turn, forms the basis for understanding the unimolecular and bimolecular reactions of these excited species. In this section, we shall consider the photochemical properties of a broad assortment of d^{10} systems.

(i) Intraligand excited states

It is difficult, a priori, to predict the reactivity of intraligand excited states of coordination compounds. While it seems reasonable to expect ligand-centered reactions, the influence of the metal on such processes can be substantial and result in net photochemistry which differs from that of the free ligand. Lacking useful generalizations, we shall simply describe some examples that illustrate the range of intraligand photoreactions undergone by d^{10} complexes.

Numerous studies have dealt with the excited state interactions of d^{10} metalloporphyrin complexes with a variety of organic and inorganic substrates [74–76]. Much of the recent interest in these systems has arisen from the desire to develop efficient photochemical routes for the cleavage of water into H_2 and O_2. With their intense intraligand π_L–π_L^* absorption bands in the visible and UV regions, their generally high efficiency of intersystem crossing to the lowest intraligand π_L–π_L^* triplet state, and their ability to undergo ring-centered oxidation and reduction at convenient potentials, d^{10} metalloporphyrins possess many of the attributes of an ideal photosensitizer for water splitting reactions.

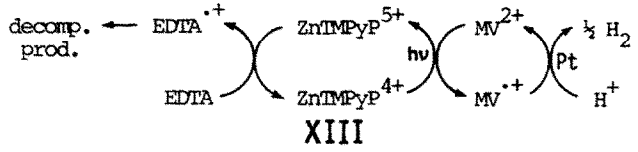

XIII

Scheme 1.

In the model system outlined in Scheme 1, visible irradiation of an acidic aqueous solution of zinc(II) *meso*-tetrakis(*N*-methyl-4-pyridyl)porphine (**XIII**) in the presence of methylviologen dication, MV^{2+}, results in the oxidative quenching of the long-lived $^3(\pi_L-\pi_L^*)$ state of the metalloporphyrin [76]. Although the quantum efficiency for formation of the redox products can be appreciable (80%), rapid back-electron transfer between these species can drastically reduce their photostationary state concentrations. To circumvent this problem, a sacrificial reductant such as EDTA is used to intercept the oxidized metalloporphyrin prior to its recombination with $MV^{\cdot+}$. In the presence of colloidal platinum as catalyst, the $MV^{\cdot+}$ species is reoxidized to MV^{2+} with concomitant reduction of protons to H_2. Methylviologen thus plays the role of an electron relay in this system.

An alternative strategy for H_2 production, which avoids the use of a relay, is summarized in Scheme 2 [76]. Here the $^3(\pi_L-\pi_L^*)$ state of $ZnTMPyP^{4+}$ undergoes reductive quenching by EDTA. Reduction of H^+ to H_2 is then coupled, via the platinum catalyst, to regeneration of the parent metalloporphyrin. Systems in which d^{10} metalloporphyrins sensitize the oxidation of H_2O to O_2 have also been reported [77,78].

Flash photolysis studies reveal that both singlet and triplet $(\pi_L-\pi_L^*)$ states of zinc(II) porphyrins are quenched with comparable rates by nitroaromatic compounds and other electron-acceptor substrates [79–81]. While quenching occurs in both polar and non-polar solvents, different transients are generated in the two environments. In polar media, both singlet and triplet excited states of the metalloporphyrin yield free ions which recombine at nearly diffusion-controlled rates. In non-polar solvents, however, triplet-state quenching affords long-lived triplet exciplexes which relax directly to the ground states of the metalloporphyrin and quencher. In some cases, ternary exciplexes composed of the metalloporphyrin and two quencher molecules have been detected [79].

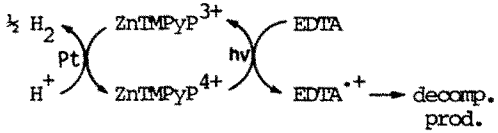

Scheme 2.

Electronic energy transfer provides another pathway by which intraligand excited states of d^{10} metalloporphyrins can interact with added substrates. Bimolecular energy transfer from the $^3(\pi_L-\pi_L^*)$ state of a tin(IV) porphyrin complex to thioindigo, for example, results in *cis–trans* isomerization of the organic molecule [82]. An interesting example of intramolecular energy transfer occurs in Zn(II)–porphyrin complexes containing an extraplanar isomerizable ligand such a *cis*- (**XIV**) or *trans*-4-stilbazole (**XV**) [83]. Light

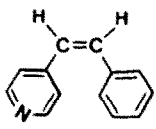

XIV

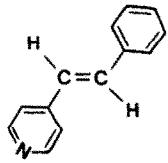

XV

absorbed by the long-wavelength intraligand transitions of the metalloporphyrin was found to promote efficient geometrical isomerization of the coordinated azastilbene. The high quantum yields (greater than unity in some cases) for this transformation were attributed to a quantum chain process that arose from reversible intramolecular energy transfer between the $^3(\pi_L-\pi_L^*)$ state of the metalloporphyrin and the azastilbene ligand. The key features of the proposed mechanism are summarized in eqns. (2)–(6), where MP represents the metalloporphyrin, and *cis*-stil and *trans*-stil denote the isomeric 4-stilbazoles. Reverse energy transfer in eqn. (5) coupled with rapid ligand exchange in eqn. (6) account for the high quantum yields observed:

$$\text{MP}-(\textit{cis}\text{-stil}) \xrightarrow{h\nu} {}^1\text{MP}^*-(\textit{cis}\text{-stil}) \longrightarrow {}^3\text{MP}^*-(\textit{cis}\text{-stil}) \quad (2)$$

$${}^3\text{MP}^*-(\textit{cis}\text{-stil}) \longrightarrow \text{MP}-({}^3\textit{trans}\text{-stil}^*) \quad (3)$$

$$\text{MP}-({}^3\textit{trans}\text{-stil}^*) \longrightarrow \text{MP}-(\textit{trans}\text{-stil}) \text{ or } \text{MP}-(\textit{cis}\text{-stil}) \quad (4)$$

$$\text{MP}-({}^3\textit{trans}\text{-stil}^*) \longrightarrow {}^3\text{MP}^*-(\textit{trans}\text{-stil}) \quad (5)$$

$${}^3\text{MP}^*-(\textit{trans}\text{-stil}) + \textit{cis}\text{-stil} \longrightarrow {}^3\text{MP}^*-(\textit{cis}\text{-stil}) + \textit{trans}\text{-stil} \quad (6)$$

Metal dithizonates form an extensive class of photochromic compounds [84,85]. Among these are the d^{10} complexes of general formula $M(HDz)_2$, where M is divalent zinc, cadmium or mercury, and HD_z^- is the singly deprotonated anion of diphenylthiocarbazone. Under dim light, benzene solutions of the complexes appear orange owing to an intense intraligand absorption band at about 500 nm. Irradiation into this band shifts the absorption to around 600 nm with a consequent change in color to dark blue. Regeneration of the original color occurs in the dark and the system can be cycled repeatedly between the "orange" and "blue" forms. This

photochromic behavior results from the reversible, intramolecular ligand isomerization process depicted in eqn. (7):

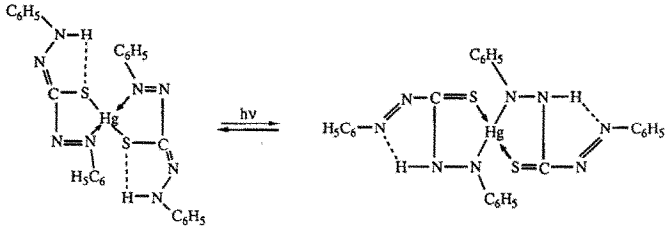

orange blue (7)

Originally, it was suggested that each dithizonate ligand in the complex can undergo photoisomerization independently [85]. The later finding that the quantum yield for the conversion in eqn. (7) approaches unity discounts this possibility (since a maximum yield of 0.5 would result if each ligand were required to absorb a photon), and suggests instead that both ligands isomerize essentially simultaneously following light absorption [86]. Three-coordinate complexes of formula RHg(HDz), where R is a methyl, phenyl or substituted phenyl group, display spectral and photochromic properties similar to those just described [87,88].

Photoexcitation of the intraligand transitions in zinc(II), cadmium(II) and mercury(II) bis(dithiolene) complexes leads to some interesting photochemical behavior [15,16,89]. In ethanol or tetrahydrofuran, the major photoprocess between 275–405 nm is reversible breakage of a metal–sulfur bond, accompanied a portion of the time by *cis–trans* isomerization about the central C–C bond of the dithiolene ligand (Scheme 3).

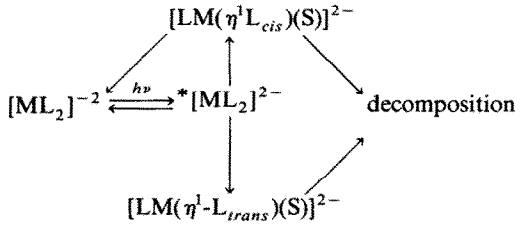

Scheme 3. ($L = S_2C_2(CN)_2^{2-}$, S = Solvent)

In addition, laser flash photolysis studies reveal that photoionization becomes a significant pathway for the zinc(II) and cadmium(II) complexes at lower excitation wavelengths (248 and 308 nm). This latter process, which affords the metal dithiolene radical anion and a solvated electron (eqn. (8)), is proposed to originate from a CTTS excited state populated via internal conversion from a higher lying intraligand state:

$$M[S_2C_2(CN)_2]_2^{2-} \xrightarrow{h\nu} M[S_2C_2(CN)_2]_2^{-} + e^- \text{ (solv)} \qquad (8)$$

(ii) Metal-to-ligand charge transfer excited states

Metal-to-ligand charge transfer excited states of Cu(I)–polypyridine complexes formally contain a copper(II) center bound to a polypyridine radical anion. While these states can be expected to exhibit oxidizing properties by virtue of the vacant *d* orbital (hole) on the divalent metal, evidence of such behavior is currently lacking. In contrast, several studies have established that the presence of a loosely held π^* electron on the coordinated radical anion causes MLCT states to function as strong reductants. Exemplary in this regard is $Cu(dmp)_2^+$ (see **V**), for which a $Cu(dmp)_2^{2+}/{}^*Cu(dmp)_2^+$ potential of -1.2 V vs. the standard hydrogen electrode (SHE) can be estimated [90–92]. Irradiation into the MLCT band of this complex in the presence of a series of cobalt(III) complexes leads to the net production of copper(II) and cobalt(II) species in 1 : 1 stoichiometry. Two limiting mechanisms for this photoredox process have been suggested. The first, outlined in Scheme 4A, involves the formation of a ground state $Cu(dmp)_2^+ \cdots Co^{III}$ complex which, upon illumination, undergoes outer-sphere electron transfer. Alternatively, in Scheme 4B, electron transfer occurs during a diffusional encounter of photoexcited $Cu(dmp)_2^+$ and the cobalt(III) substrate. In both mechanisms, separation of the nascent $Cu(dmp)_2^{2+} \cdots Co^{II}$ redox pair into the final products competes with unproductive back-electron transfer.

The issue of static (Scheme 4A) vs. dynamic (Scheme 4B) quenching of MLCT excited states was addressed in a study of the effect of nitroaromatic quenchers on the charge transfer luminescence of $Cu(dpp)_2^+$ (see **V**) in CH_2Cl_2 [93]. Quenching data obeyed the Stern–Volmer kinetic expression given by

$$\tau^0/\tau = 1 + k_q[\text{quencher}] \tag{9}$$

where τ and τ^0 represent emission lifetimes in the presence and absence respectively of the quencher, and k_q is the second-order quenching rate constant. This key finding establishes that quenching occurs via a dynamic

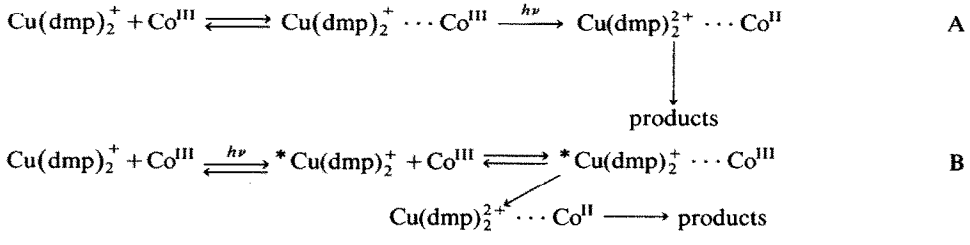

Scheme 4.

TABLE 5

Quenching of $Cu(dpp)_2^+$ luminescence by nitroaromatic compounds [a] (from ref. 93)

Quencher	k_q (M^{-1} s^{-1})	$E_{1/2}$ (V)	ΔG_{el} [b] (kcal)
p-Dinitrobenzene	1.1×10^{10}	−1.18	−5.3
m-Dinitrobenzene	3.2×10^{9}	−1.37	−0.9
4,4′-Dinitrobiphenyl	2.9×10^{8}	−1.48	1.6
1-Chloro-4-nitrobenzene	2.9×10^{7}	−1.58	3.9
Nitrobenzene	2.4×10^{6}	−1.76	8.1

[a] All measurements were made in CH_2Cl_2; $E_{1/2}$ values are referenced to the ferrocene couple. [b] See eqn. (10).

mechanism. Table 5 contains a compilation of k_q values, quencher reduction potentials, $E_{1/2}$, and free energies of oxidative quenching, ΔG_{el}. The last quantity can be calculated from the relationship

$$\Delta G_{el}(\text{kcal}) = 23.06\left[(-1.41\text{ V}) - E_{1/2}\right] \tag{10}$$

where −1.41 V is the estimated potential of the $Cu(dpp)_2^{2+}/{}^*Cu(dpp)_2^+$ couple vs. ferrocene. The approach of k_q to the diffusion limit when $\Delta G_{el} < 0$ and the monotonic fall off in k_q as ΔG_{el} becomes increasingly positive are characteristic traits of electron transfer quenching.

As illustrated in Fig. 15, a more complicated relationship between ΔG_{el} and k_q obtains for quenching of the MLCT excited state of $Cu(dpp)_2^{2+}$ by a series of tris(β-diketonate)chromium(III) complexes [93]. While k_q initially exhibits the expected decrease (note the solid line in Fig. 15) from the diffusion-limited plateau as ΔG_{el} increases toward zero, it levels off again at a value of about 10^7 M^{-1} s^{-1} in the endoergic region. This second plateau has been attributed to a change in the predominant mechanism of quenching from electron transfer to exchange (collisional) energy transfer:

$$^*Cu(dpp)_2^+ + Cr^{III} \longrightarrow Cu(dpp)_2^+ + {}^*Cr^{III} \tag{11}$$

The chromium(III) complexes possess low lying ligand field excited states of doublet spin multiplicity whose energies are nearly insensitive to the identity of the β-diketonate ligand. Energy transfer to these excited states occurs with very similar rate constants, thus accounting for the lower plateau. In general, quenching via energy transfer to form a *d–d* excited state is expected to level off at a lower value of k_q than quenching via electron transfer because of the more exacting orbital overlap requirement of the former process [94].

Because of their intense MLCT absorption bands, which can be tuned over a substantial portion of the visible region, and the strongly reducing nature of the corresponding MLCT excited states, several Cu(I)–polypyri-

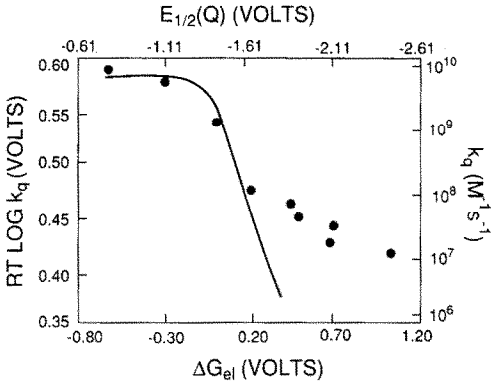

Fig. 15. Correlation between the rate constant (k_q) for quenching of the MLCT excited state of Cu (dpp)$_2^+$ by tris(β-diketonate)chromium(III) complexes and the free energy of electron transfer (ΔG_{el}). $E_{1/2}$(Q) is the reduction potential of the chromium(III) quencher referenced to the ferrocene couple. The solid line represents the predicted correlation if only electron transfer quenching occurs. Reprinted with permission from ref. 93. Copyright 1985 American Chemical Society.

dine complexes have been examined as sensitizers in solar energy conversion systems [95,96]. Illumination of an n-type ZnO photoanode coated with Cu(dpp)$_2^+$, for example, produces a sensitized photocurrent whose action spectrum tracks the absorption spectrum of the complex. As illustrated in Fig. 16, this behavior reflects the ability of the MLCT excited state of Cu(dpp)$_2^+$ to inject an electron into the conduction band of the semiconductor. Regeneration of the original complex results from the reaction of Cu(dpp)$_2^{2+}$ with the reducing agent hydroquinone (H_2Q). Measurement of

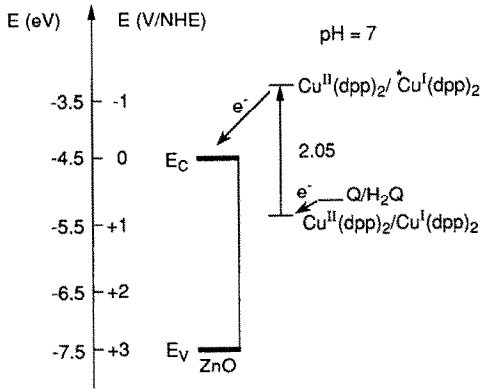

Fig. 16. Energy levels of n-ZnO, Cu(dpp)$_2^+$ and Q/H_2Q in 1.5 M KCl and 5×10^{-3} M H_2Q at pH 7. E_v and E_c denote the positions of the valence and conduction bands respectively. From ref. 95.

the light-to-electricity quantum efficiency yields a value of the order of 1–2% for excitation near 410 nm. The width of the sensitized spectral region can be quite impressive in such systems, extending out to 700 nm in the case of $Cu(tpp)_2^+$ (see V) adsorbed onto ZnO.

High intensity pulsed-laser irradiation of $Cu(dpp)_2^+$ in deaerated CH_2Cl_2 solution causes a rapid bleaching of the MLCT absorption band [97]. The intensity dependence of bleaching provides evidence for a two-photon photochemical reaction. Analysis of the photolyte reveals the formation of $Cu(dpp)_2^{2+}$ and Cl^-, the latter species presumably arising from the reductive cleavage of a C–Cl bond in the solvent. These findings were interpreted in terms of the mechanistic sequence outlined in eqns. (12)–(15):

$$Cu(dpp)_2^+ \overset{h\nu}{\rightleftharpoons} {}^*Cu(dpp)_2^+ \tag{12}$$

$${}^*Cu(dpp)_2^+ \overset{h\nu}{\rightleftharpoons} {}^{**}Cu(dpp)_2^+ \tag{13}$$

$$[{}^{**}Cu(dpp)_2^+]CH_2Cl_2 \longrightarrow Cu(dpp)_2^{2+} + {}^{\cdot -}CH_2Cl_2 \tag{14}$$

$${}^{\cdot -}CH_2Cl_2 \longrightarrow Cl^- + \text{other products} \tag{15}$$

Sequential absorption of two photons by $Cu(dpp)_2^+$ leads initially to the population of the relatively long-lived MLCT excited state (eqn. (12)) and then to the production of a higher lying reactive excited state (denoted by two asterisks in eqn. (13)). Outer-sphere electron transfer between the latter state and a molecule of CH_2Cl_2 in the second coordination sphere (eqn. (14)) yields the oxidized complex and a solvent radical anion which subsequently releases Cl^- (eqn. (15)).

There are indications that MLCT excitation may induce chemical reactions of olefins bound to copper(I) [98]. Irradiation of $Cu(C_2H_4)^+$ in ethylene-saturated ethanol, for instance, produces hexane via a mechanism thought to involve a σ-bonded Cu–alkyl species (Scheme 5) [99]. Formally, such a species arises from the photoinduced transfer of an electron from Cu^+ to the coordinated olefin. Likewise, MLCT excitation would generate the proposed Cu–alkyl intermediate in the *cis–trans* isomerization of 1,5-cyclooctadiene bound to copper(I) [99].

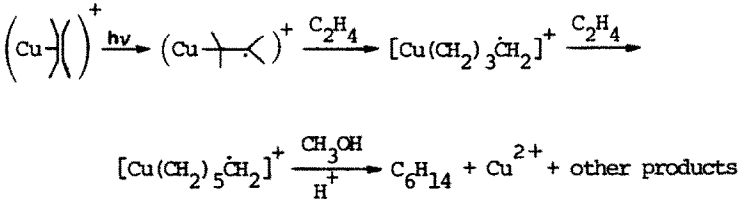

Scheme 5.

(iii) Charge-transfer-to-solvent excited states

Consistent with the view that CTTS transitions in metal complexes result in an outward flow of electron density to the surrounding solution medium [39–45], irradiation into the CTTS band of anionic copper(I) complexes leads to photoelectron production with concomitant oxidation of the metal center. As exemplified by the behavior of $CuCl_3^{2-}$, CTTS excitation produces a primary geminate pair, $\overline{CuCl_3^-,e^-}$ (eqn. (16)), which can either recombine or separate slightly to afford a secondary geminate pair, $CuCl_3^-,e^-$ (eqn. (17)). The latter species, in turn, may recombine or undergo diffusive separation into the bulk solvent (eqn. (18)). Direct detection of the hydrated electron by laser flash photolysis provides compelling support for this reaction sequence [39]. In the presence of a good electron scavenger such as the hydrogen ion or N_2O, the secondary pair can be intercepted (eqn. (19)). Scavenging by protons in acidic solution is of some interest from the standpoint of energy storage, since the hydrogen atoms generated ultimately lead, either by direct combination (eqn. (20)) or via a copper hydride intermediate (eqn. (21)), to the production of hydrogen gas [100,101]:

$$CuCl_3^{2-} \overset{h\nu}{\rightleftharpoons} \overline{CuCl_3^-,e^-} \quad (16)$$

$$\overline{CuCl_3^-,e^-} \rightleftharpoons CuCl_3^-,e^- \quad (17)$$

$$CuCl_3^-,e^- \longrightarrow CuCl_3^- + e^- \quad (18)$$

$$CuCl_3^-,e^- + H^+ \longrightarrow CuCl_3^- + H^\cdot \quad (19)$$

$$H^\cdot + H^\cdot \longrightarrow H_2 \quad (20)$$

$$HCuCl_3^{2-} + H^+ \longrightarrow H_2 + CuCl_3^- \quad (21)$$

Photoelectron production also occurs upon CTTS excitation of an equilibrium mixture of the cationic complexes $Cu(NH_3)_3^+$ and $Cu(NH_3)_2^+$ [44]. In the presence of added NH_4^+, the photogenerated electron is scavenged to produce H_2 (eqn. (22)):

$$Cu(NH_3)_3^+ + NH_4^+ \overset{h\nu}{\longrightarrow} Cu(NH_3)_4^{2+} + 1/2\ H_2 \quad (22)$$

As noted earlier, a photoionization pathway in metal dithiolenes (eqn. (8)) has been attributed to population of a CTTS excited state [89].

(iv) Ligand-to-metal charge transfer excited states

Ligand-to-metal charge transfer excited states in coordination compounds formally contain a reduced metal center and an oxidized ligand radical. Each of these species is potentially capable of reacting with its geminate partner (back-electron transfer), with itself (bimolecular disproportionation

or coupling), or with some other component (solvent, added substrate) present in the system. The photopolymerization of tetrahydrofuran solutions containing small amounts of Ag^+, Cu^+ or Tl^+ salts exemplifies such behavior [47,102]. Light-induced ligand-to-metal charge transfer within a ground state THF–metal ion complex generates the reduced metal and the tetrahydrofuran radical cation (**XVI**) (eqn. (23)):

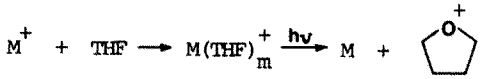

XVI (23)

Aggregation of the zerovalent metal atoms occurs essentially irreversibly and thereby prevents unproductive back-electron transfer between the primary photoproducts. Subsequent reaction of **XVI** produces intermediates **XVII** (eqn. (24)) and **XVIII** (eqn. (25)), both of which are known to initiate cationic polymerization (eqn. (26)):

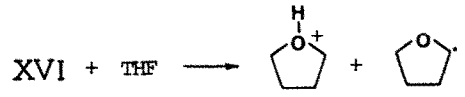

XVII (24)

XVIII (25)

XVII and/or **XVIII** $\xrightarrow{THF}$ polymer (26)

A similar mechanism obtains for the photoinduced addition of acetonitrile to norbornene in the presence of Ag^+ or Tl^+ salts [103,104]. Ligand-to-metal charge transfer excitation of a pre-formed metal–norbornene complex generates the norbornene radical cation (eqn. (27)) which then abstracts a hydrogen atom from acetonitrile (eqn. (28)). The resulting $^{\cdot}CH_2CN$ radical initiates a chain process (eqns. (29) and (30)) that yields the observed addition product:

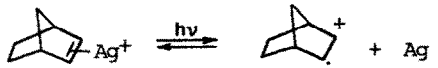

(27)

(28)

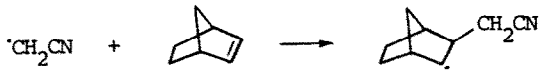

(29)

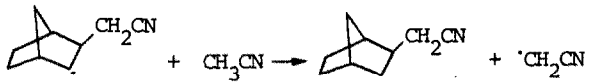

(30)

Analogous solvent–norbornene adducts are formed in propionitrile and methanol solutions.

Irradiation into the LMCT absorption bands of $Sn(N_3)_6^{2-}$ and $Pb(N_3)_6^{2-}$ results in the reductive elimination of two azide radicals [46]

$$M^{IV}(N_3)_6^{2-} \xrightarrow{h\nu} M^{II}(N_3)_4^{2-} + 2N_3^{\cdot} \tag{31}$$

The latter species decompose to molecular nitrogen and nitrogen atoms

$$N_3^{\cdot} \longrightarrow N_2 + N^{\cdot} \tag{32}$$

It remains to be determined whether the overall reaction occurs via a simultaneous two-electron reduction of the metal by the two azide groups or via two sequential one-electron steps involving tin(III) or lead(III) intermediates.

Photolysis of d^{10} metal complexes containing η^1-bonded carbocyclic rings causes the initial cleavage of the metal–ring bonds (eqns. (33)–(35)) [48,49]:

$$Cd(\eta^1\text{-}C_6H_5)_2 \xrightarrow{h\nu} Cd + 2^{\cdot}C_6H_5 \tag{33}$$

$$Hg(\eta^1\text{-}C_5H_5)_2 \xrightarrow{h\nu} Hg + 2^{\cdot}C_5H_5 \tag{34}$$

$$Sn(\eta^1\text{-}C_5H_5)_4 \xrightarrow{h\nu} Sn(\eta^1\text{-}C_5H_5)_3 + {}^{\cdot}C_5H_5 \tag{35}$$

The resulting organic radicals undergo coupling, atom abstraction, or other characteristic reactions. While detailed spectral studies of these systems are lacking, the observed photochemistry suggests the involvement of LMCT excited states in the primary photochemical step.

Likewise, the photoproducts that result from the novel rearrangement processes of methylenecyclopropanes irradiated in the presence of $Cu(F_3CSO_3)$ support a mechanism involving LMCT excitation of an olefin–Cu ground state complex [105]. As illustrated in eqn. (36), charge transfer induces "photocupration" or the transformation of an η^2-copper(I) olefin complex into an η^1-β-copper(I) carbenium ion:

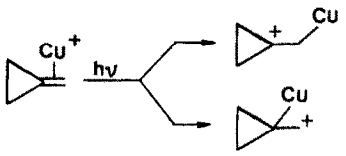

(36)

Skeletal rearrangments can ensue via well-precedented reactions of these types of carbenium ions. Photocupration has also been invoked as a possible mechanism in copper(I)-mediated olefin photocycloaddition reactions [98,106].

(v) Ligand-to-ligand charge transfer excited states

Very little is known about the reactivity of LLCT excited states in d^{10} complexes. Nevertheless, we can anticipate that the electron transfer nature of this type of state should facilitate redox chemistry. A precedent for such behavior is provided by the d^8 complex Pt(bipy)(tdt), which undergoes photooxidation in chloroform [107]:

$$Pt(bipy)(tdt) + CHCl_3 \xrightarrow{h\nu} Pt(bipy)(tdt)^+ + Cl^- + {}^{\cdot}CHCl_2 \qquad (37)$$

There is also some evidence that LLCT excited states can sensitize singlet oxygen production, but the mechanism of this process is unclear [108].

(vi) Interconfigurational metal-centered excited states

It has been suggested that the interconfigurational metal-centered excited state arising from a $3d \rightarrow 4s$ transition in anionic copper(I) complexes (e.g. $CuCl_3^{2-}$) possesses many of the traits of a CTTS state (see Section C(iii)) [45]. Thus the $3d^9 4s^1$ state contains an electron in a spherical $4s$ orbital that is larger and more diffuse than the $3d$ orbital it occupied in the ground state. With its greater radial extension, the $4s$ electron interacts strongly with the solution environment and, for a portion of the time, can escape into the bulk solvent. According to this picture, $3d^9 4s^1$ and CTTS represent complementary orbital descriptions of the primary geminate pair formed upon UV excitation of these anionic complexes (see eqn. (16)). This interesting proposal has merit and deserves further experimental testing.

Visible irradiation of $Pd_2(dppm)_3$ in the presence of CH_2Cl_2 leads to the quantitative formation of a methylene-bridged dimer [58]:

$$Pd_2(dppm)_3 + CH_2Cl_2 \xrightarrow{h\nu} Pd_2(\mu\text{-}CH_2)(dppm)_2Cl_2 + dppm \qquad (38)$$

This reaction, which is thought to originate from the metal-centered $4d^9 5p^1$ excited state, formally involves a net four-electron oxidation of the dimeric unit. Analogous redox chemistry occurs for the monomeric complex $Pd(PPh_3)_4$:

$$Pd(PPh_3)_4 + C_6H_5Cl \xrightarrow{h\nu} \textit{trans}\text{-}Pd(PPh_3)_2(C_6H_5)Cl \qquad (39)$$

(vii) σ–a_π *excited states*

Copper(I) complexes of general formula CuP_mX, where P is a monodentate or polydentate arylphosphine, X is a uninegative group such as Cl^-, Br^- or BH_4^-, and $m = 1$–3 do not undergo efficient intramolecular photodecomposition when irradiated directly into their spin-allowed σ–a_π absorption bands [61,109]. Instead, the dominant process following photoexcitation is intersystem crossing to the $^3(\sigma$–$a_\pi)$ state, whose microsecond lifetime facilitates bimolecular interactions with suitable substrates in solution. Photoisomerization of *cis*- (**XIX**) and *trans*-piperylene (**XX**)

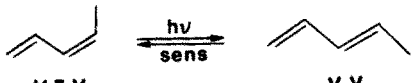

XIX XX (40)

can, for example, be sensitized with high quantum efficiency by Cu(diphos)BH_4 (**XI**) and Cu(prophos)BH_4 (**XII**) [62]. For each complex, sensitization is accompanied by quenching of the emissive $^3(\sigma$–$a_\pi)$ excited state and the two processes occur with identical Stern–Volmer kinetics. Measurements of the *trans*/*cis* diene ratio at the photostationary state can be used to estimate the triplet state energy (E_T) as 60–61 kcal for Cu(diphos)BH_4 and 61 kcal or more for Cu(prophos)BH_4; other evidence suggests that 66–67 kcal is a reasonable value for the latter complex. In both cases, the $^3(\sigma$–$a_\pi)$ state lies above the $^3(\pi$–$\pi^*)$ excited states of the piperylenes. Collectively, the results support the assignment of intermolecular energy transfer as the primary mechanism for quenching and sensitization in these systems.

The observation that Cu$(PPh_2Me)_3Cl$, Cu$(PPh_3)_2BH_4$ and Cu(prophos)BH_4 function as efficient photosensitizers for the valence isomerization of norbornadiene (**XXI**) to quadricyclene (**XXII**)

XXI XXII (41)

whereas Cu(diphos)BH_4 is ineffective in this role [61,109,110] also can be explained in terms of electronic energy transfer [62]. This process is exoergic for Cu$(PPh_2Me)_3Cl$ and Cu$(PPh_3)_2BH_4$ as donors ($E_T \approx 76$ kcal) and the diene as acceptor ($E_T \approx 72$ kcal). Triplet–triplet energy transfer from Cu(prophos)BH_4 to NBD, however, is endoergic by 3–4 kcal; nonetheless, the long lifetime of the $^3(\sigma$–$a_\pi)$ excited state (Table 4) permits the complex to acquire sufficient thermal energy from the surroundings to overcome this deficit and energy transfer can still occur with high quantum efficiency. In

the case of Cu(diphos)BH_4, the endoergicity rises to about 9 kcal and energy transfer can no longer compete with other deactivation processes of the $^3(\sigma-a_\pi)$ state.

ACKNOWLEDGEMENT

Acknowledgement is made to the Donors of The Petroleum Research Fund, administered by the American Chemical Society, for partial support of our work in the subject area of this article.

REFERENCES

1 G. Wilkinson, R.D. Gillard and J.A. McCleverty (Eds.), Comprehensive Coordination Chemistry, Vol. 5, Pergamon, Oxford, 1987.
2 F.A. Cotton and G. Wilkinson, Advanced Inorganic Chemistry, 5th edn., Wiley-Interscience, New York, 1988.
3 F. Basolo and R.G. Pearson, Mechanisms of Inorganic Reactions, 2nd edn., Wiley, New York, 1967, Chapters 2 and 3.
4 H.-H. Schmidtke, in H.O.A. Hill and P. Day (Eds.), Physical Methods in Advanced Inorganic Chemistry, Interscience, London, 1968, Chapter 4.
5 V. Balzani and V. Carassiti, Photochemistry of Inorganic Compounds, Academic Press, New York, 1970, Chapter 5.
6 L.S. Forster, in A.W. Adamson and P. Fleischauer (Eds.), Concepts of Inorganic Photochemistry, Wiley-Interscience, New York, 1975, Chapter 1.
7 G.A. Crosby, J. Chem. Educ., 60 (1983) 791.
8 D.D. Chapman and E.R. Schmittou, in G. Wilkinson, R.D. Gillard and J.A. McCleverty (Eds.), Comprehensive Coordination Chemistry, Vol. 6, Pergamon, Oxford, 1987, Chapter 59.
9 M. Grätzel (Ed.), Energy Resources through Photochemistry and Catalysis, Academic Press, New York, 1983.
10 G.A. Crosby, Acc. Chem. Res., 8 (1975) 231.
11 T.N. Sorrell and A.S. Borovik, J. Am. Chem. Soc., 108 (1986) 2479.
12 T.N. Sorrell, A.S. Borovik and C.-C. Chen, Inorg. Chem., 25 (1986) 590.
13 T.N. Sorrell and A.S. Borovik, Inorg. Chem., 26 (1987) 1957.
14 M. Gouterman, in D. Dolphin (Ed.), The Porphyrins, Vol. 3, Part A, Academic Press, New York, 1978, Chapter 1.
15 A. Fernandez and H. Kisch, Chem. Ber., 117 (1984) 3102.
16 H. Kisch, J. Bücheler, A. Fernandez, H. Görner and N. Zeug, Sci. Papers Inst. Phys. Chem. Res. (Jpn.), 78 (1984) 178.
17 D.J. Casadonte, Jr., and D.R. McMillin, J. Am. Chem. Soc., 109 (1987) 331.
18 G.A. Crosby, R.G. Highland and K.A. Truesdell, Coord. Chem. Rev., 64 (1985) 41.
19 M.T. Buckner and D.R. McMillin, J. Chem. Soc., Chem. Commun., (1978) 759.
20 A.A. Del Paggio and D.R. McMillin, Inorg. Chem., 22 (1983) 691.
21 C.O. Dietrich-Buchecker, P.A. Marnot, J.-P. Sauvage, J.R. Kirchoff and D.R. McMillin, J. Chem. Soc., Chem. Commun., (1983) 513.
22 A.K. Ichinaga, J.R. Kirchoff, D.R. McMillin, C.O. Dietrich-Buchecker, P.A. Marnot and J.-P. Sauvage, Inorg. Chem., 26 (1987) 4290.

23 M.T. Buckner, T.G. Matthews, F.E. Lytle and D.R. McMillin, J. Am. Chem. Soc., 101 (1979) 5846.
24 G. Blasse and D.R. McMillin, Chem. Phys. Lett., 70 (1980) 1.
25 R.A. Rader, D.R. McMillin, M.T. Buckner, T.G. Matthews, D.J. Casadonte, R.K. Lengel, S.B. Whittaker, L.M. Darmon and F.G. Lytle, J. Am. Chem. Soc., 103 (1981) 5906.
26 P.A. Breddels, P.A.M. Berdowski, G. Blasse and D.R. McMillin, J. Chem. Soc., Faraday Trans. 2, 78 (1982) 595.
27 J.R. Kirchoff, R.E. Gamache, Jr., M.W. Blaskie, A.A. Del Paggio, R.K. Lengel and D.R. McMillin, Inorg. Chem., 22 (1983) 2380.
28 G. Blasse, P.A. Breddels and D.R. McMillin, Chem. Phys. Lett., 109 (1984) 24.
29 D.J. Casadonte and D.R. McMillin, Inorg. Chem., 26 (1987) 3950.
30 C.E.A. Palmer and D.R. McMillin, Inorg. Chem., 26 (1987) 3837.
31 M.W. Blaskie and D.R. McMillin, Inorg. Chem., 19 (1980) 3519.
32 K.V. Goodwin and D.R. McMillin, Inorg. Chem., 26 (1987) 875.
33 D.R. McMillin, J.R. Kirchoff and K.V. Goodwin, Coord. Chem. Rev., 64 (1985) 83.
34 C.E.A. Palmer, D.R. McMillin, C. Kirmaier and D. Holten, Inorg. Chem., 26 (1987) 3167.
35 S.E.J. Bell and J.J. McGarvey, Chem. Phys. Lett., 124 (1986) 336.
36 J.J. McGarvey, S.E.J. Bell and J.N. Bechara, Inorg. Chem., 25 (1986) 4325.
37 J.J. McGarvey, S.E.J. Bell and K.C. Gordon, Inorg. Chem., 27 (1988) 4003.
38 N.A.P. Kane-Maguire, L.L. Wright, J.A. Guckert and W.S. Tweet, Inorg. Chem., 27 (1988) 2905.
39 D.D. Davis, K.L. Stevenson and C.R. Davis, J. Am. Chem. Soc., 100 (1978) 5344.
40 C.R. Davis and K.L. Stevenson, Inorg. Chem., 21 (1982) 2514.
41 K.S. Kurtz and K.L. Stevenson, Proc. Indiana Acad. Sci., 94 (1985) 187.
42 O. Horvath and S. Papp, J. Photochem., 30 (1985) 47.
43 A. Horvath and S. Papp, J. Photochem., 24 (1984) 331.
44 T.F. Braish, R.E. Duncan, J.J. Harber, R.L. Steffen and K.L. Stevenson, Inorg. Chem., 23 (1984) 4072.
45 K.L. Stevenson, J.L. Braun, D.D. Davis, K.S. Kurtz and R.I. Sparks, Inorg. Chem., 27 (1988) 3472.
46 A. Vogler, C. Quett, A. Paukner and H. Kunkely, J. Am. Chem. Soc., 108 (1986) 8263.
47 M.E. Woodhouse, F.D. Lewis and T.J. Marks, J. Am. Chem. Soc., 104 (1982) 5586.
48 A.M. Osman, A.I. Khodair, A.A. Abdel-Wahab and A.M. El-Khawaga, Can. J. Chem., 57 (1979) 1923.
49 P.J. Barker, A.G. Davies and M.-W. Tse, J. Chem. Soc., Perkin Trans. 2, (1980) 941.
50 V.J. Koester, Chem. Phys. Lett., 32 (1975) 575.
51 K.A. Truesdell and G.A. Crosby, J. Am. Chem. Soc., 107 (1985) 1787.
52 R.G. Highland and G.A. Crosby, Chem. Phys. Lett., 119 (1985) 454.
53 R.G. Highland, J.G. Brummer and G.A. Crosby, J. Phys. Chem., 90 (1986) 1593.
54 S.A. Payne, A.B. Goldberg and D.S. McClure, J. Chem. Phys., 78 (II) (1983) 3688.
55 K. Tanimura, W.A. Sibley and L.G. DeShazer, Phys. Rev. B, 31 (1985) 3980.
56 A. Vogler and H. Kunkely, Chem. Phys. Lett., 150 (1988) 135.
57 A. Vogler and H. Kunkely, J. Am. Chem. Soc., 108 (1986) 7211.
58 J.V. Caspar, J. Am. Chem. Soc., 107 (1985) 6718.
59 P.D. Harvey, W.P. Schaefer and H.B. Gray, Inorg. Chem., 27 (1988) 1101.
60 P.D. Harvey and H.B. Gray, J. Am. Chem. Soc., 110 (1988) 2145.
61 P.A. Grutsch and C. Kutal, J. Am. Chem. Soc., 101 (1979) 4228.

62 B. Liaw, S.W. Orchard and C. Kutal, Inorg. Chem., 27 (1988) 1311.
63 D.J. Fife, K.W. Morse and W.M. Moore, J. Photochem., 24 (1984) 249.
64 D.J. Fife and K.W. Morse, Inorg. Chem., 23 (1984) 1545.
65 P.A. Grutsch and C. Kutal, J. Am. Chem. Soc., 99 (1977) 6460.
66 K.L. Rogozhin, A.N. Rodionov, S.G. Smirnov, D.N. Shigorin, E.M. Panov and K.A. Kochesdov, Bull. Acad. Sci. USSR, Div. Chem. Sci., (1977) 949 (English translation).
67 G.V. Ratovskii, A.M. Panov, O.A. Yakutina, Y.I. Sukhorukov and E.N. Tsvetkov, J. Gen. Chem. USSR, 48 (1978) 1394 (English translation).
68 A.I. Bokanov and B.I. Stepanov, J. Gen. Chem. USSR, 49 (1979) 1036 (English translation).
69 D.P. Segers, M.K. DeArmond, P.A. Grutsch and C. Kutal, Inorg. Chem., 23 (1984) 2874.
70 M.A.S. Goher, Naturwissenschaften, 62 (1975) 237.
71 H.D. Hardt and A. Pierre, Inorg. Chim. Acta., 25 (1977) L59.
72 E. Eitel, D. Oelkrug, W. Hiller and J. Strähle, Z. Naturforsch., Teil B, 35 (1980) 1247.
73 N.P. Rath, E. Holt and K. Tanimura, J. Chem. Soc., Dalton Trans., (1986) 2303.
74 F.R. Hopf and D.G. Whitten, in D. Dolphin (Ed.), The Porphyrins, Vol. 2, Part B, Academic Press, New York, 1978, Chapter 6.
75 M.-C. Richoux, in A. Harriman and M.A. West (Eds.), Photogeneration of Hydrogen, Academic Press, London, 1982, p. 39.
76 A. Harriman, J. Photochem., 29 (1985) 139.
77 E. Bogarello, K. Kalyanasundaram, Y. Okuno and M. Grätzel, Helv. Chim. Acta, 64 (1981) 1937.
78 P.A. Christensen, A. Harriman, G. Porter and P. Neta, J. Chem. Soc., Faraday Trans. 2, 80 (1984) 1451.
79 J.K. Roy and D.G. Whitten, J. Am. Chem. Soc., 93 (1971) 7093.
80 J.K. Roy and D.G. Whitten, J. Am. Chem. Soc., 94 (1972) 7162.
81 J.K. Roy, F.A. Carroll and D.G. Whitten, J. Am. Chem. Soc., 96 (1974) 6349.
82 G.M. Wyman, B.M. Zarnegar and D.G. Whitten, J. Phys. Chem., 77 (1973) 2584.
83 D.G. Whitten, P.D. Wildes and C.A. DeRosier, J. Am. Chem. Soc., 94 (1972) 7811.
84 L.S. Meriwether, E.C. Breitner and C.L. Sloan, J. Am. Chem. Soc., 87 (1965) 4441.
85 L.S. Meriwether, E.C. Breitner and N.B. Colthup, J. Am. Chem. Soc., 87 (1965) 4448.
86 C. Geosling, A.W. Adamson and A.R. Gutierrez, Inorg. Chim. Acta, 29 (1978) 279.
87 A.T. Hutton and H.M.N.H. Irving, J. Chem. Soc., Chem. Commun., (1979) 1113.
88 A.T. Hutton and H.M.N.H. Irving, J. Chem. Soc., Dalton Trans., (1982) 2299.
89 A. Fernandez, H. Görner and H. Kisch, Chem. Ber., 118 (1985) 1936.
90 D.R. McMillin, M.T. Buckner and B.T. Ahn, Inorg. Chem., 16 (1977) 943.
91 B.T. Ahn and D.R. McMillin, Inorg. Chem., 17 (1978) 2253.
92 B.T. Ahn and D.R. McMillin, Inorg. Chem., 20 (1981) 1427.
93 R.E. Gamache, Jr., R.A. Rader and D.R. McMillin, J. Am. Chem. Soc., 107 (1985) 1141.
94 V. Balzani, L. Moggi, M.F. Manfrin, F. Bolletta and G.S. Laurence, Coord. Chem. Rev., 15 (1975) 321.
95 N.A. Vante, V. Ern, P. Chartier, C.O. Dietrich-Buchecker, D.R. McMillin, P.A. Marnot and J.-P. Sauvage, Nouv. J. Chim., 7 (1983) 3.
96 P.A. Breddels, G. Blasse, D.J. Casadonte and D.R. McMillin, Ber. Bunsenges. Phys. Chem., 88 (1984) 572.
97 R.M. Berger, D.R. McMillin and R.F. Dallinger, Inorg. Chem., 26 (1987) 3802.
98 R.G. Salomon, Tetrahedron, 39 (1983) 485.
99 D. Geiger and G. Ferraudi, Inorg. Chim. Acta, 101 (1985) 197.
100 G. Ferraudi, Inorg. Chem., 17 (1978) 1370.

101 K.L. Stevenson, D.M. Kaehr, D.D. Davis and C.R. Davis, Inorg. Chem., 19 (1980) 781.
102 M.E. Woodhouse, F.D. Lewis and T.J. Marks, J. Am. Chem. Soc., 100 (1978) 996.
103 J.W. Bruno, T.J. Marks and F.D. Lewis, J. Am. Chem. Soc., 103 (1981) 3608.
104 J.W. Bruno, T.J. Marks and F.D. Lewis, J. Am. Chem. Soc., 104 (1982) 5580.
105 R.G. Salomon and M.F. Salomon, J. Am. Chem. Soc., 98 (1976) 7454.
106 R.G. Salomon and J.K. Kochi, J. Am. Chem. Soc., 96 (1974) 1137.
107 A. Vogler and H. Kunkely, J. Am. Chem. Soc., 103 (1981) 1559.
108 L. Kumar, K.H. Puthraya and T.S. Srivastava, Inorg. Chim. Acta, 86 (1984) 173.
109 D.J. Fife, W.M. Moore and K.W. Morse, J. Am. Chem. Soc., 107 (1985) 7077.
110 S.W. Orchard and C. Kutal, Inorg. Chim. Acta, 64 (1982) L95.